derived in terms of the CFSE's, gives a reasonable sorting of the cases where it is applicable (Table I), use of MOSE's alone does not give as good a picture.[22]

A structural sorting using the χ^A, χ^B indexes is understandable in terms of current ideas concerning site preference energies in molecules.[18,24] Given a set of atomic charges $\{q_i^\xi\}$ for the orbitals i (s, p, d) located on the symmetry inequivalent atoms (ξ) in a structure, the total energy will depend on the function $\sum_{i,\xi} q_i^\xi H_{ii}^\xi$, where H_{ii}^ξ is the relevant valence orbital ionization potential. The most stable structure will be the one with optimal matching of $\{q_i^\xi\}$ and $\{H_{ii}^\xi\}$ to give the lowest energy. In general, this will occur when the most electronegative atoms (largest H_{ii}) occupy the sites of highest charge. Since energetically they are more important than ligand–metal d interactions, the ligand–metal s,p interactions should analogously control the charge distribution and hence the site preferences. The gross structural sorting is then explicable in principle on these grounds, although, at present, we do not understand the exact location of the dividing lines. In addition, because of the impotence of d orbitals in determining these preferences, we can see why the number of electrons in these orbitals is immaterial in the display of Figure 1 (but, of course, vital to a CFT discussion). The finer details of the structures close to the boundaries, where the CFT methodology does appear to dominate, are also much more in keeping with the general idea that the d-orbital effects are small compared to s and p ones in this area.

An additional point concerning the relative sizes of the two types of interactions is associated with Jahn–Teller distortions in Cu^{II}- and Mn^{III}-containing spinels. These are best viewed as structural perturbations of the spinel structure itself, rather than leading to the generation of a completely different structural type. Such Jahn–Teller effects also appear to give rise to a relatively small structural perturbation in AB_2 systems[15] when viewed via structural mapping.

Although we have perhaps downplayed the importance of d orbitals and their occupation in this paper, it is vital to recognize that this view has only been advanced for the coordination number problem. There is ample evidence that this manifold of orbitals[25] and their electron occupancy is of tremendous importance in controlling angular geometry, relative bond lengths, ligand site preferences, reactivity, and many other facets of molecular structure.[18]

Finally it will be interesting to see if these ideas, developed for solids, can be extended to the molecular area. In recent years, most progress in understanding the structures of solids has resulted from the flow of ideas in the reverse direction.[26,27]

Acknowledgment. We thank the donors of the Petroleum Research Fund administered by the American Chemical Society for their partial support of this research and the National Science Foundation for their support under Grants NSF DMR 8019741 and NSF CHE 7826579. We also acknowledge useful discussion and correspondence with D. S. McClure.

Registry No. $FeAl_2O_4$, 12068-49-4; $MgAl_2O_4$, 1302-67-6; $CoAl_2O_4$, 1333-88-6; $MnAl_2O_4$, 12068-52-9; $CuAl_2O_4$, 12042-92-1; $CdAl_2O_4$, 12252-16-3; $NiAl_2O_4$, 12004-35-2; $MnGa_2O_4$, 12064-15-2; $CdGa_2O_4$, 12139-12-7; $MgGa_2O_4$, 12064-13-0; $CoGa_2O_4$, 12139-60-5; $FeGa_2O_4$, 12062-71-4; $CuGa_2O_4$, 12053-83-7; $NiGa_2O_4$, 12064-17-4; $ZnMn_2O_4$, 12163-55-2; $CdMn_2O_4$, 12050-21-4; $CoMn_2O_4$, 12139-69-4; $MgMn_2O_4$, 12163-24-5; $CuMn_2O_4$, 12019-04-4; $NiMn_2O_4$, 12057-90-8; VMn_2O_4, 12163-54-1; $FeMn_2O_4$, 12332-30-8; $TiMn_2O_4$, 12032-93-8; $SnMn_2O_4$, 12209-43-7; $CrMn_2O_4$, 12410-51-4.

(24) Hoffmann, R.; Howell, J. M.; Muetterties, E. L. *J. Am. Chem. Soc.* **1976**, *98*, 2484.

(25) Although we traditionally call these "d orbitals", if the local symmetry is lower than cubic, then they will in fact contain admixture of s and p orbitals. In this sense then higher energy orbitals also play a crucial role in determining even these properties.

(26) See, for example, the articles in ref 7c.

(27) Burdett, J. K. *Nature London* **1979**, *279*, 121.

Structures of $[(Ph_3C_3)M(PPh_3)_2]^+X^-$ Complexes. An Experimental and Theoretical Study of Ring-Whizzing

Carlo Mealli,[1a] Stefano Midollini,[1a] Simonetta Moneti,[1a] Luigi Sacconi,*[1a] Jerome Silvestre,[1b] and Thomas A. Albright*[1b,c]

Contribution from the Instituto di Stereochimica di Coordinazione del C.N.R., Instituto di Chimica Generale e Inorganica dell' Universita', 50132 Firenze, Italy, and the Department of Chemistry, University of Houston, Houston, Texas 77004. *Received February 27, 1981. Revised Manuscript Received August 15, 1981*

Abstract: Complexes of the formula $[(Ph_3C_3)M(PPh_3)_2]X$, where M = Ni, Pd and X = ClO_4, PF_6, have been prepared by the reaction of (ethylene)$M(PPh_3)_2$ with triphenylcyclopropenium perchlorate or hexafluorophosphate. Complete X-ray analysis has been carried out for $[(Ph_3C_3)Ni(PPh_3)_2]PF_6$ (**1**), $[(Ph_3C_3)Pd(PPh_3)_2]ClO_4$ (**2**), and $[(Ph_3C_3)Pd(PPh_3)_2]PF_6 \cdot C_6H_6$ (**3**). The crystal data are as follows: (**1**) a = 15.815 (4) Å, b = 13.781 (4) Å, c = 12.764 (4) Å, α = 114.06 (9)°, β = 95.92 (9)°, γ = 97.74 (9)°, Z = 2, space group $P\bar{1}$; (**2**) a = 11.115 (4) Å, b = 35.486 (9) Å, c = 12.584 (4) Å, β = 104.49 (7)°, Z = 4, space group $P2_1/n$; (**3**) a = 12.130 (5) Å, b = 23.863 (7) Å, c = 18.669 (6) Å, β = 91.45 (8)°, Z = 4, space group $P2_1/n$. The structures were refined to R values 0.079, 0.079, and 0.065 for **1**, **2**, and **3**, respectively. These three structures, along with a previously determined one where M = Pt, X = PF_6, **4**, show a progressive movement of the $(Ph_3P)_2M$ unit over the face of the cyclopropenium cation. In other words, these structures chart the reaction path for going from one η^2 geometry, where the $(Ph_3P)_2M$ unit is positioned below one carbon–carbon bond, to an equivalent η^2 geometry. The movement of the $(PPh_3)_2M$ group is accompanied by rotation, as well as a number of other geometrical changes. A potential surface for this ring-whizzing motion was determined by molecular orbital calculations of the extended Hückel type. The calculations mimic the geometrical details experimentally found and provide an electronic rationale for the observed distortions. The calculations and observed structures are in agreement with the McIver–Stanton theorem which regulates the symmetry of potential surfaces. The effect of substitution on the cyclopropenium ring and of changing the phosphines to other ligands on the potential surface is also discussed.

Ring-Whizzing, a type of fluxionality where an ML_n unit migrates inside the periphery of a cyclic polyene, has been extensively studied by NMR methods.[2] Activation energies throughout the entire range of dynamic NMR (ca. 7–22 kcal/mol)

0002-7863/82/1504-0095$01.25/0

have been measured. Theoretical work on this problem in the organometallic and main-group areas has been rather scarce.[3] Organic analogues, sigmatropic rearrangements, have been thoroughly investigated.[4] We present three structures of the (cyclopropenium)ML_2 cation type which were determined by X-ray diffraction. Specifically compounds **1**–**3**[5] were categorized

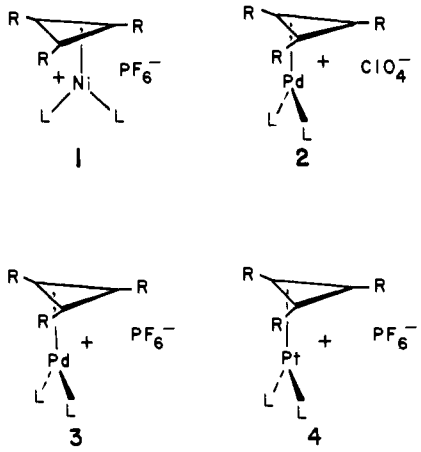

where R = Ph and L = PPh_3. An analogous Pt structure, **4**, has been determined by McClure and Weaver.[6] We contend that these structures define a substantial portion of the reaction path for ring-whizzing in a d^{10} (cyclopropenium)ML_2 system.

The ability to chart a reaction path from X-ray structures is predicted on a relatively low potential for distortion to the transition state. Variations of intra- and intermolecular contacts among a group of closely related molecules then will create geometrical changes. It is assumed that the molecules will be pushed in the direction of lowest energy, i.e., the reaction coordinate in a multidimensional potential surface. This approach was pioneered and beautifully elaborated by Bürgi, Dunitz, and Murray-Rust.[7] Examples of nucleophilic substitution, electrophilic substitution, and the Cope rearrangement have been documented[7] from the organic and main-group areas. Guggenberger and Muetterties[8] have studied polytopal rearrangements in ML_n complexes. We are aware of no other work in this area in the transition-metal organometallic field.

Chart I

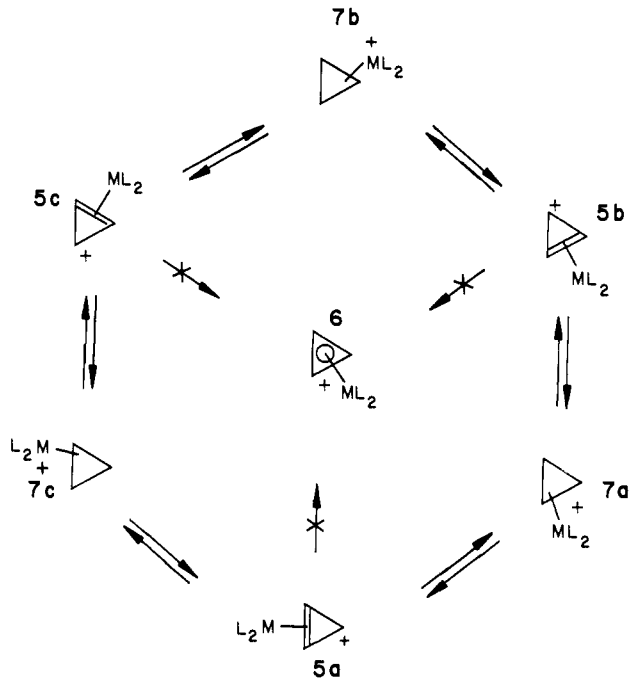

McIver and Stanton have given[9] a set of rules concerning the symmetry of potential surfaces. The four structures lend experimental support to this theorem. Chart I shows three possible way points for ring-whizzing in the d^{10} (cyclopropenium)ML_2 system. Let us say that the ground state for the complex (in the gas phase) is η^2; i.e., the ML_2 group is coordinated to and lies somewhere above a carbon–carbon bond in the cyclopropenium polyene. **5a**–**c** then represent the three equivalent ground-state geometries. An attractive structure for the transition state would be an η^3 geometry, **6**. However, this would mean that three valleys (taking into consideration that there is free rotation at the η^3 geometry; vide infra) exit from the transition state. This is forbidden according to the McIver–Stanton rules.[9] There must be a set of three points which lie lower in energy and serve as transition states. These are represented in Chart I by **7a**–**c**. **6** actually serves as an energy maximum. We shall show that the structures of **1**–**4** correspond to points between the extremes of **5** and **7**. In none of the structures does the $M(PPh_3)_2$ group attain η^3 bonding as in **6**; therefore, we offer direct experimental support to the McIver–Stanton rules. Molecular orbital calculations of the extended Hückel type[10] are also used to detail the potential surface illustrated in Chart I as well as to define the mode of bonding between the ML_2 and cyclopropenium units.

One might have expected that the η^3 geometry would have been favored as the ground state. Several examples of η^3 (cyclopropenium)ML_3 have been reported,[11] as well as an example of η^1-coordination.[12] An alternative view takes the η^2 geometry as a way point toward an oxidative insertion into the C–C bond of

(1) CNR, Universita', Firenze. (b) University of Houston. (c) Camille and Henry Dreyfus Teacher-Scholar 1979–1984.

(2) For reviews, see: (a) Jackman, L. M.; Cotton, F. A. "Dynamic Nuclear Magnetic Resonance Spectroscopy"; Academic Press: New York, 1975; pp 377–488. (b) Deganello, G. "Transition Metal Complexes of Cyclic Polyolefins"; Academic Press: New York, 1979. (c) Mann, B. E. *Prog. Nucl. Magn. Reson. Spectrosc.* **1977**, *11*, 95. (d) Fedorov, L. A. *Russ. Chem. Rev. (Engl. Transl.)* **1973**, *42*, 678. (e) Faller, J. W. *Adv.* Organomet. *Chem.* **1977**, *16*, 211.

(3) (a) Anh, N. T.; Elian, M.; Hoffmann, R. *J. Am. Chem. Soc.* **1978**, *100*, 110. (b) Albright, T. A.; Hoffmann, R.; Tse, Y.-C.; D'Ottavio, T *Ibid.* **1979**, *101*, 3812. (c) Albright, T. A.; Geiger, W. E., Jr.; Moraczewski, J.; Tulyathan, B., *Ibid.* **1981**, *103*, 4787. (d) Albright, T. A. *J. Organomet. Chem.* **1980**, *92*, 159. (e) Hofmann, P.; Albright, T. A. *Angew. Chem.* **1980**, 92, 747. (f) Hofmann, P. *Z. Naturforsch. B: Anorg. Chem., Org. Chem.* **1977**, *33B*, 251. (g) Mingos, D. M. P.; Nurse, C. R. *J. Organomet. Chem.* **1980**, *184*, 281. Mingos, D. M. P. *J. Chem. Soc., Dalton Trans.* **1977**, *31*. (h) Herndon, W. C. *J. Am. Chem. Soc.* **1980**, *102*, 1538. (i) Brauer, D. J.; Krüger, C. *Inorg. Chem.* **1977**, *16*, 884. (j) Su, C.-C. *J. Am. Chem. Soc.* **1971**, *93*, 5653. (k) McKinney, M. A.; Haworth, D. T. *J. Chem. Educ.* **1980**, *57*, 110.

(4) For review of the theory and experiments, see: Woodward, R. B.; Hoffmann, R. "The Conservation of Orbital Symmetry"; Verlag Chemie: Weinheim, 1970; pp 114–140. Anh, N. T. "Die Woodward-Hoffmann Regeln und ihre Anwendung"; Verlag Chemie: Weinheim, 1972; pp 59–112.

(5) A communication on the structure of **1** has appeared: Mealli, C.; Midollini, S.; Moneti, S.; Sacconi, L. *Angew. Chem.* **1980**, *92*, 967.

(6) McClure, M. D.; Weaver, D. L. *J. Organomet. Chem.* **1973**, *54*, C59.

(7) Bürgi, H.-B. *Angew. Chem.* **1975**, *87*, 461; *Angew. Chem., Int. Ed. Engl.* **1975**, *14*, 460. Dunitz, J. D. "X-ray Analysis and the Structure of Molecules"; Cornell University Press: Ithaca, NY, 1979; pp 301–390. Murray-Rust, P. In "Molecular Structure by Diffraction Methods"; Stutton, L. E., Truter, M. R., Eds.; Bartholomew Press: Dorking, England, 1978; Vol. 6, pp 154–182.

(8) Muetterties, E. L.; Guggenberger, L. J. *J. Am. Chem. Soc.* **1974**, *96*, 1748. Muetterties, E. L. *Tetrahedron* **1974**, *30*, 1595. Guggenberger, L. J.; Muetterties, E. L. *J. Am. Chem. Soc.* **1976**, *98*, 7221. See also: Kepert, D. L. *Prog. Inorg. Chem.* **1977**, *23*, 1; **1978**, *24*, 179; **1979**, *25*, 41. Favas, M. C.; Kepert, D. L. *Ibid.* **1980**, *27*, 325, and references therein for related material.

(9) (a) Stanton, R. E.; McIver, J. W. Jr., *J. Am. Chem. Soc.* **1975**, *97*, 3632; McIver, J. W., Jr. *Ibid.* **1972**, *94*, 2625; *Acc. Chem. Res.* **1974**, *7*, 72. (b) Bouman, T. D.; Duncan, C. D.; Trindle, C. *Int. J. Quantum Chem.* **1977**, *11*, 399. Trindle, C.; Bouman, T.; Datta, S.; Duncan, C. in "Computers in Chemical Education and Research"; Ludena, E. V., Sabelli, N. H., Wahl, A. C. Eds.; Plenum Press: New York, 1977; pp 261–290. (c) Pechukas, P. *J. Chem. Phys.* **1976**, *64*, 1516. (d) Nourse, J. G. *J. Am. Chem. Soc.* **1980**, *102*, 4883.

(10) Hoffmann, R. *J. Chem. Phys.* **1963**, *39*, 1397. Hoffmann, R.; Lipscomb, W. N. *Ibid.* **1962**, *36*, 3179, 3489; **1962**, *37*, 2872.

(11) (a) Mealli, C.; Midollini, S.; Moneti, S.; Sacconi, L. *J. Organomet. Chem.* **1981**, *205*, 273. (b) Chiang, T.; Kerber, R. C.; Kimball, S. D.; Lauher, J. W. *Inorg. Chem.* **1979**, *18*, 1687. (c) Weaver, D. L.; Tuggle, R. M. *J. Am. Chem. Soc.* **1969**, *91*, 6506; *Inorg. Chem.* **1971**, *10*, 2599. (d) Tuggle, R. M.; Weaver, D. L. *Ibid.* **1971**, *10*, 1504.

(12) Gompper, R.; Bartmann, E.; Noth, H. *Chem. Ber.* **1979**, *112*, 218.

Table I. Crystal Data and Data Collection Details

	$[(PPh_3)_2Ni(C_3Ph_3)]PF_6$	$[(PPh_3)_2Pd(C_3Ph_3)]PF_6 \cdot C_6H_6$	$[(PPh_3)_2Pd(C_3Ph_3)]ClO_4$
mol formula	$C_{57}H_{45}F_6NiP_3$	$C_{63}H_{51}F_6P_3Pd$	$C_{57}H_{45}ClO_4P_2Pd$
mol wt	995.62	1121.42	997.79
a, *b*, *c*, Å	15.815 (4), 13.781 (4), 12.764 (4)	12.130 (5), 23.863 (7), 18.669 (6)	11.115 (4), 35.486 (9), 12.584 (5)
α, β, γ, deg	114.06 (9), 95.92 (9), 97.74 (9)	90, 91.45 (8), 90	90, 104.49 (7), 90
d_{obsd} (by flot), g cm^{-3}	1.30	1.36	1.35
d_{calcd}, g cm^{-3}	1.33	1.38	1.38
V, Å^3	2478.34	5402.16	4805.58
Z	2	4	4
space group	$P\bar{1}$	$P2/n$	$P2_1/n$
abs coeff (Mo Kα), cm^{-1}	5.36	4.76	5.38
color	red	reddish brown	reddish brown
habit and faces	prism, {001}, {100}, {010}	prism {010}, {101}, {011}	prism {001}, {011}, {$\bar{1}$01}
dimensions, mm	0.1 × 0.12 × 0.175	0.15 × 0.275 × 0.30	0.1 × 0.125 × 0.40
(Mo Kα)	0.71069 (monochromatized)	0.71069 (monochromatized)	0.71069 (monochromatized)
method	θ–2θ	θ–2θ	θ–2θ
scan speed, deg/s	0.07	0.07	0.07
scan width, deg	0.84	0.84	0.84
background measuring time	half of the scan time for all compounds		
standards	three reflections measured every 120′ for all compounds		
max stand dev	8%	2%	4%
2θ limits, deg	$5 \leq 2\theta \leq 40$	$5 \leq 2\theta \leq 48$	$5 \leq 2\theta \leq 44$
no. of data used ($I \geq 3\sigma(I)$)	2908	4783	3564

the cyclopropenium fragment. Several metal complexes of this latter type have been categorized,[13] and an excellent theoretical discussion has been given by Jemmis and Hoffmann.[14] The ML_2 complexes described here are 11-electron systems at either η^3 or η^2. We expected that the unique nature of the ML_2 fragment orbitals would present a continuum of energetically attainable geometries as is the case in other (polyene)ML_2 systems.[3b,c,e,15]

Experimental Section

Reagents. The complexes $(C_2H_4)Ni(PPh_3)_2$[16] and $(C_2H_4)Pd(PPh_3)_2$[17] and the cyclopropenyl salts $(Ph_3C_3)ClO_4$[18] and $(Ph_3C_3)PF_6$[18] were prepared by methods previously described.

Preparation of the Complexes. All the reactions were carried out under dry nitrogen with deoxygenated dry solvents, and the complexes were dried in a stream of dry nitrogen. The yields were generally more than 75%.

$[(Ph_3C_3)Ni(PPh_3)_2]X$ (X = ClO_4, PF_6). the appropriate triphenylcyclopropenyl salt (1 mmol) in 20 mL of methanol was added to a solution of 1 mmol of $(C_2H_4)Ni(PPh_3)_2$ in 20 mL of benzene. On addition of 20 mL of 1-butanol and slow evaporation of the solvent, red crystals were formed. The compounds can be recrystallized from methylene chloride 1-butanol. Anal. Calcd for $C_{57}H_{45}F_6NiP_3$: C, 68.76; H, 4.76. Found: C, 68.46; H, 4.47. Calcd for $C_{57}H_{45}ClNiO_4P_2$: C, 72.06; H, 4.77, Ni, 6.18. Found: C, 71.80; H, 5.29; Ni, 6.06.

$[(Ph_3C_3)Pd(PPh_3)_2]PF_6 \cdot C_6H_6$. $(C_3Ph_3)PF_6$ (1 mmol) in 15 mL of methylene chloride was added to a solution of 1 mmol of $(C_2H_4)Pd(PPh_3)_2$ in 20 mL of benzene. On addition of 20 mL of 1-butanol, a reddish-brown oil separated which slowly crystallized. Anal. Calcd for $C_{57}H_{45}F_6PdP_3 \cdot C_6H_6$: C, 67.47; H, 4.58. Found: C, 66.37; H, 4.76.

$[(Ph_3C_3)Pd(PPh_3)_2]ClO_4$. The complex was prepared with a method analogous to that used for the nickel derivatives. Anal. Calcd for $C_{57}H_{45}ClO_4PdP_2$: C, 68.62; H, 4.55. Found: C, 68.63; H, 4.97.

NMR Measurements. ^{13}C NMR spectra of $[(Ph_3C_3)Pd(PPh_3)_2]PF_6$ were obtained in CD_2Cl_2 solutions on a Varian CFT 20 spectrometer at 20 MHz with proton noise decoupling and a deuterium lock. The resonance of the cyclopropenyl ring carbons were at 95.4 ppm (triplet, $^2J_{^{13}C-^{31}P}$ = 9.4 Hz) at 20 °C and at 96.2 ppm (triplet, $^2J_{^{13}C-^{31}P}$ = 9.2 Hz).

Computational Methods. The extended Hückel calculations used the atomic parameters previously given[19] with the modified Wolfsberg–Helmholz approximation.[20] The calculations on $(C_3H_3)Ni(Ph_3)_2^+$ employed C–C, C–H, Ni–P, and P–H bond lengths of 1.41, 1.09, 2.15, and 1.42 Å, respectively. The P–Ni–P and Ni–P–H angles were set at 110° and 123.1°, respectively. At η^3 the Ni–cyclopropenium ring distance was 1.717 Å. Calculations on $(C_3H_3)Ni(CO)_2^+$ utilized Ni–C and C–O lengths of 1.82 and 1.14 Å, respectively. The C–Ni–C and Ni–C–O angles were 110° and 180°, respectively. All other geometrical parameters were identical with those in the phosphine case.

Collection and Reduction of X-ray Intensity Data. All three compounds were studied by using a Philips PW 1100 computer-controlled diffractometer. The radiation used was Mo Kα monochromatized with a flat graphite crystal. The procedure to obtain cell parameters from a number of "hunted" and centered reflections was that previously described.[21] The refinement of a set of 15–20 reflections was carefully selected in the θ range 10–11°. Details of the crystal data and data collections are given in Table I. After correction for background, the standard deviations of the intensities, I, were calculated by using instability factors of 0.03 for all compounds. The data were corrected for the Lorentz–polarization effect, and absorption corrections were applied to the F_o values. The transmission factors are in the ranges 0.98–0.96, 0.92–0.76, and 0.97–0.93 for **1**, **2**, and **3**, respectively.

Solution and Refinement of the Structures. The calculations were carried out by using the SHELX 76 package of programs implemented on a SEL 32/70 computer. Atomic scattering factors and dispersion corrections were taken from the literature.[22] All of the structures were solved by combining Patterson and direct methods in the early stages and F_o and ΔF Fourier syntheses after the location of the metal and phosphorus atoms. Full matrix least-squares refinements were based on F_o, the function minimized being $\sum W(|F_o| - |F_c|)^2$, where $w = 1/\sigma^2(F_o)$. The agreement factors are defined as $R = \sum||F_o| - |F_c||/\sum|F_o|$ and $R_w = [\sum(w|F_o| - |F_c|)^2/\sum w|F_o|^2]^{1/2}$. Throughout the refinement, the phenyl rings were treated as rigid groups of D_{6h} symmetry. Hydrogen atoms were introduced at calculated positions (d_{C-H} = 0.95 Å) in the late stages of refinement, but were not refined. Metal, phosphorus, and chlorine atoms were treated anisotropically after the first cycles of refinement.

In all structures the anions (PF_6^- or ClO_4^-) were found to be affected by disorder. Careful examination of ΔF maps calculated in the late stages of refinement for **1** and **3** enabled us to determine a second quasi-octahedral model for the PF_6 anions concentric with the main ones but

(13) (a) Tuggle, R. M.; Weaver, D. L. *J. Am. Chem. Soc.* **1970**, *92*, 5523; *Inorg. Chem.* **1972**, *11*, 2237. (b) Frisch, P. D.; Khare, G. P. *Ibid.* **1979**, *18*, 781. Posey, R. G.; Khare, G. P.; Frisch, P. D. *J. Am. Chem. Soc.* **1977**, *99* 4863. Frisch, P. D.; Posey, R. G.; Khare, G. P. *Inorg. Chem.* **1978**, *17*, 402. (c) Bailey, P. M.; Keasey, A.; Maitlis, P. M. *J. Chem. Soc., Chem. Commun.* **1977**, 178. (d) Hoberg, H.; Krause-Göing, R.; Krüger, C.; Sekutowski, J. C. *Angew. Chem.* **1977**, *89*, 179.

(14) Jemmis, E. D.; Hoffmann, R. *J. Am. Chem. Soc.* **1980**, *102*, 2570.

(15) (a) Radonovich, L. J.; Koch, F. J.; Albright, T. A. *Inorg. Chem.* **1980**, *19*, 3373. (b) Byers, L. R.; Dahl, L. F. *Ibid.* **1980**, *19*, 277. (c) Albright, T. A.; Hoffmann, R. *Chem. Ber.* **1978**, *111*, 1578. (d) Mingos, D. M. P. *J. Chem. Soc., Dalton Trans.* **1977**, 602. Mingos, D. M. P.; Forsyth, M. I.; Welch, A. J. *Ibid.* **1978**, 1363.

(16) Giannocaro, P.; Sacco, A.; Vasapollo, G. *Inorg. Chim. Acta* **1979**, *37*, L455.

(17) Visser, A.; Van der Linde, R.; De Youngh, R. O. *Inorg. Synth.* **1976**, *16*, 127.

(18) Breslow, R.; Chang, H. W. *J. Am. Chem. Soc.* **1961**, *83*, 2374.

(19) Albright, T. A.; Hoffmann, R.; Thibeault, J. C.; Thorn, D. L. *J. Am. Chem. Soc.* **1979**, *101*, 3801.

(20) Ammeter, J. H.; Bürgi, H.-B., Thibeault, J. C.; Hoffmann, R. *J. Am.* Chem. *Soc.* **1978**, *100*, 3686.

(21) Mealli, C.; Midollini, S.; Sacconi, L. *Inorg. Chem.* **1975**, *14*, 2513, and references therein.

(22) "International Tables for X-ray Crallography"; Kynoch Press: Birmingham,; Vol. IV.

Table II. Final Atomic Parameters for $[(Ph_3C_3)Ni(PPh_3)_2]PF_6$

(a) Anisotropically Refined Atoms

atom	x	y	z	U_{11}	U_{22}	U_{33}	U_{12}	U_{13}	U_{23}
Ni	2632 (1)	2348 (1)	3484 (1)	46 (1)	54 (1)	42 (1)	19 (1)	8 (1)	21 (1)
P1	1189 (2)	2154 (3)	3333 (3)	48 (2)	58 (3)	39 (2)	16 (2)	11 (2)	22 (2)
P2	2933 (2)	691 (3)	2640 (3)	56 (3)	57 (3)	62 (3)	25 (2)	16 (2)	22 (2)
P3	2525 (3)	5627 (4)	112 (4)	83 (4)	110 (4)	77 (4)	21 (3)	21 (3)	46 (3)

(b) Isotropically Refined Atoms

atom	x	y	z	U, Å²	atom	x	y	z	U, Å²
F1	1965 (12)	4426 (18)	−471 (17)	128 (6)	C21	5260 (7)	−40 (8)	3579 (8)	124 (7)
F2	2558 (11)	5718 (13)	1378 (16)	106 (6)	C22	5805 (7)	375 (8)	3004 (8)	122 (7)
F3	3109 (14)	6813 (16)	786 (17)	132 (8)	C23	5479 (7)	873 (8)	2337 (8)	132 (7)
F4	2546 (14)	5490 (17)	−1158 (19)	149 (9)	C24	4608 (7)	957 (8)	2244 (8)	95 (5)
F5	3426 (10)	5236 (12)	−51 (12)	100 (4)	C25	28 (6)	1066 (8)	1066 (8)	61 (4)
F6	1714 (14)	6083 (18)	503 (18)	154 (9)	C26	2340 (6)	617 (6)	495 (8)	72 (4)
F7	1542 (13)	4976 (17)	−329 (16)	72 (6)	C27	2210 (6)	186 (6)	−718 (8)	98 (5)
F8	2302 (14)	5963 (17)	−968 (20)	86 (7)	C28	2392 (6)	−833 (6)	−1362 (8)	90 (5)
F9	2738 (16)	5279 (19)	1193 (22)	95 (8)	C29	2704 (6)	−1421 (6)	−791 (8)	95 (5)
F10	2738 (24)	4346 (34)	−456 (33)	185 (14)	C30	2834 (6)	−991 (6)	423 (8)	75 (4)
F11	3367 (25)	6452 (31)	369 (30)	164 (16)	C31	2398 (6)	−179 (8)	3229 (6)	59 (4)
F12	2056 (22)	6642 (26)	314 (26)	156 (14)	C32	1882 (6)	−1202 (8)	2558 (6)	73 (4)
C61	3018 (8)	3862 (10)	4381 (11)	55 (4)	C33	1447 (6)	−1767 (8)	3098 (6)	95 (5)
C62	3686 (8)	3458 (10)	3726 (10)	49 (4)	C34	1528 (6)	−1310 (8)	4309 (6)	92 (5)
C63	3670 (8)	3379 (10)	4728 (10)	48 (3)	C35	2043 (6)	−287 (8)	4980 (6)	92 (5)
C1	505 (5)	796 (6)	2748 (5)	43 (3)	C36	2478 (6)	278 (8)	4440 (6)	73 (4)
C2	115 (5)	405 (6)	3468 (5)	47 (3)	C37	2715 (5)	4904 (7)	4795 (6)	52 (4)
C3	−376 (5)	−643 (6)	2998 (5)	67 (4)	C38	2808 (5)	5559 (7)	4205 (6)	61 (4)
C4	−477 (5)	−1302 (6)	1807 (5)	65 (4)	C39	2512 (5)	6534 (7)	4602 (6)	83 (5)
C5	−87 (5)	−911 (6)	1086 (5)	61 (4)	C40	2121 (5)	6854 (7)	5590 (6)	76 (5)
C6	404 (5)	137 (6)	1557 (5)	53 (4)	C41	2028 (5)	6200 (7)	6181 (6)	68 (4)
C7	698 (5)	2722 (6)	2411 (7)	45 (3)	C42	2325 (5)	5783 (6)	5783 (6)	58 (4)
C8	−195 (5)	2516 (6)	2035 (7)	51 (4)	C43	4231 (5)	3566 (7)	2896 (9)	62 (4)
C9	−536 (5)	2972 (6)	1330 (7)	60 (4)	C44	3828 (5)	3605 (7)	1892 (9)	85 (5)
C10	17 (5)	3635 (6)	1001 (7)	58 (4)	C45	4314 (5)	3658 (7)	1058 (9)	120 (6)
C11	910 (5)	3841 (6)	1378 (7)	67 (4)	C46	5202 (5)	3671 (7)	1227 (9)	118 (6)
C12	1250 (5)	3385 (6)	2082 (7)	58 (4)	C47	5604 (5)	3632 (7)	2231 (9)	91 (5)
C13	890 (5)	2850 (6)	4763 (7)	48 (3)	C48	5119 (5)	3579 (7)	3065 (9)	72 (4)
C14	1323 (5)	2697 (6)	5676 (7)	63 (4)	C49	4106 (6)	3277 (7)	5725 (7)	58 (4)
C15	1150 (5)	3219 (6)	6800 (7)	67 (4)	C50	4903 (6)	2948 (7)	5678 (7)	82 (5)
C16	544 (6)	3895 (6)	7012 (7)	71 (4)	C51	5325 (6)	2834 (7)	6624 (7)	107 (6)
C17	112 (5)	4049 (6)	6099 (7)	73 (4)	C52	4950 (6)	3049 (7)	7618 (7)	106 (6)
C18	285 (5)	3526 (6)	4974 (7)	63 (4)	C53	4153 (6)	3378 (7)	7665 (7)	112 (6)
C19	4063 (7)	542 (8)	2818 (8)	65 (4)	C54	3731 (6)	3492 (7)	6719 (7)	82 (5)
C20	4389 (7)	44 (8)	3485 (8)	104 (6)					

[a] The form of the thermal ellipsoid is $\exp[-2\pi^2(U_{11}h^2a^{*2} + U_{22}k^2b^{*2} + U_{33}l^2c^{*2} + 2U_{12}hka^*b^* + 2U_{13}hla^*c^* + 2U_{23}klb^*c^*)]$. Coordinates multiplied by 10^4, temperature factors by 10. [b] Coordinates multiplied by 10^4, temperature factors by 10^3. The population parameter of atoms F1–F6 was refined to a value of 0.62 (1); the population parameter of atoms F7–F12 was constrained to be the complement to 1 of the previous value.

differently oriented. The coordinates of these secondary models were introduced and refined by fixing at 1.00, the sum of the population parameters of the two models. This treatment allowed significant but not complete rationalization of the disorder in the region of the hexafluorophosphate anions. In fact, peaks of about 0.5–0.6 e/Å³ can still be found in ΔF maps calculated at the end of the refinements. However, since the desired chemical information is contained within the cation, we expended no more effort in better fitting the disorder of these anions. We are also convinced that only data collections at low temperature can satisfactorily solve the analogous disorder problem for the perchlorate anion in structure **2**. Its refinement was terminated at $R = 0.079$ in spite of the somewhat high temperature factors for oxygen atoms. Final reliability factors for all structures were $R = 0.079$, $R_w = 0.081$ for **1**, $R = 0.063$, $R_w = 0.065$ for **3**, and $R = 0.079$, $R_w = 0.080$ for **2**. Tables II through IV report final atomic parameters for all of the compounds. Listings of F_o and F_c are available as supplementary material.

Description of the Structures

The (ethylene)$M(PPh_3)_2$ complexes react rapidly in methanol/benzene solutions at room temperature with triphenylcyclopropenium salts to give crystalline (cyclopropenium)$M(PPh_3)_2$ complexes (eq 1). Although all six combinations of M and X

$$(C_2H_4)M(PPh_3)_2 + [Ph_3C_3]X \rightarrow [(Ph_3C_3)M(PPh_3)_2]X + C_2H_4 \quad (1)$$

M = Ni, Pd; X = ClO_4, PF_6, and BPh_4

were prepared, only complexes **1–3** gave suitable crystals for an X-ray structural determination. The nickel complexes decompose slowly in the air in the solid state and rapidly in solution. The palladium complexes are fairly stable. All of the complexes were soluble in polar solvents such as methylene chloride, chloroform, and acetone.

Discrete cationic $[(Ph_3C_3)M(PPh_3)_2]^+$ (M = Ni, Pd) species are found for the three compounds studied in this paper. The two palladium derivatives differ from each other in the nature of the anion, ClO_4^- in **2** and PF_6^- in **3**, and in the presence of isolated benzene molecules encapsulated in thhe lattice of **3**. Stereoscopic views of the monoclinic $P2_1/n$ unit cells are shown in Figures 1 and 2 for compounds **3** and **2**, respectively. The platinum derivative, **4**,[6] is isostructural with **3**.

Packing forces are likely to be of great importance in determining the different geometries for **1–4**. It is, however, noteworthy to point out that no unusual short contacts are observed in any of the structures studied by us. The shortest contacts are about 3.3 Å between several carbon atoms in the phenyl rings and fluorine or oxygen atoms of the anions. The anions are affected by a certain amount of disorder, even at the end of the refinement.

The most evident structural differences are relative to the mode by which the Ph_3C_3 and $M(PPh_3)_2$ fragments are tied together. Structural deformations within the cyclopropenium unit are also

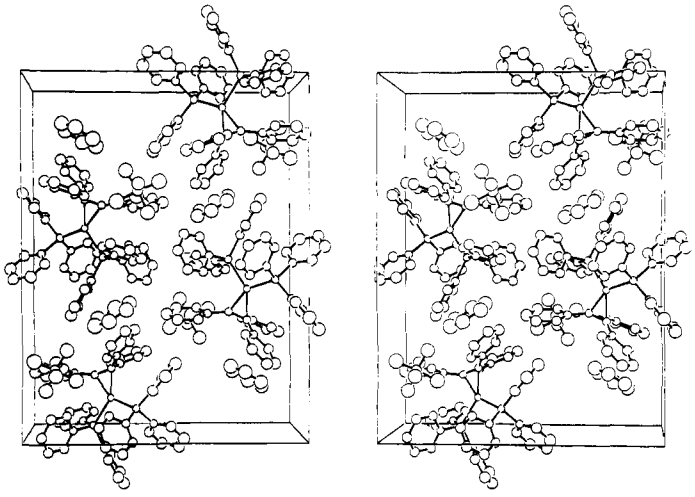

Figure 1. Stereoview of the contents of the unit cell for $[(Ph_3C_3)Pd(PPh_3)_2]PF_6 \cdot C_6H_6$.

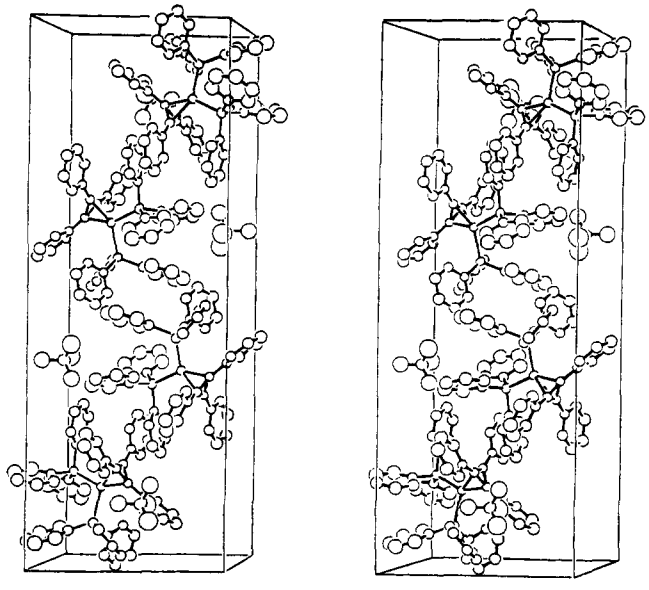

Figure 2. Stereoview of the contents of the unit cell for $[(Ph_3C_3)Pd(PPh_3)_2]ClO_4$.

observed. We shall discuss the most important geometrical details within each structure and the theoretical calculations, and finally, we shall fit the structures and calculations together to provide a description of the ring-whizzing.

Figure 3 shows overall views of compounds **1**–**3**. Selected bond distances are reported in Table V. In compound **1** (Figure 3a) the NiP_2 unit is almost perpendicular to the C_3 (cyclopropenium) ring. The dihedral angle is 88°. The NiP_2 plane almost, but not quite, bisects the C_{62}–C_{63} bond. For this reason we previously called this the upright conformation.[5] The projection of the nickel atom falls within the C_3 ring; it is about 0.60 Å from C_{61}. This carbon is also closest to the nickel atom, the distance being 1.897 (12) Å. The remaining two Ni–C distances are more the 0.1 Å longer. There is a small but significant difference between these two distances: Ni–C_{63} = 2.056 (10) Å and Ni–C_{62} = 2.009 (12) Å. In other words, the projection of the nickel atom onto the C_3 plane does not lie on the axis formed by C_{61} and the bisection of C_{62}–C_{63}. It lies off on the C_{62} side. The bond lengths within the C_3 ring are also not equal. One of them, C_{62}–C_{63}, is shorter (1.329 (21) Å) than the other two (C_{61}–C_{62} = 1.445 (18) Å and C_{61}–C_{63} = 1.425 (20) Å). The structural parameters within the $M(PPh_3)_2$ fragment are unexceptional and do not vary much in **1**–**3** once the lengthening of M–P distances on going from Ni to Pd is taken into consideration.

In the perchlorate salt of the palladium derivative, **2**, the MP_2 and C_3 planes are still approximately orthogonal. The dihedral angle is 89°. However, the projection of the metal onto the C_3 ring has slipped. It now falls almost over the C_{62}–C_{63} bond (see Figure 3b). Also the MP_2 plane has rotated approximately 14° with respect to the nickel derivative, **1**. It now forms an angle of 11° with the C_{62}–C_{63} edge. In contrast to **1**, the C_{62}–C_{63} bond is now longer than the other two. The C_{62}–C_{63}, C_{61}–C_{62} and C_{61}–C_{63} bond lengths are 1.461 (16), 1.371 (18), and 1.387 (18) Å, respectively. A reversal is also observed for the Pd–C bond lengths. The Pd–C_{61} bond length of 2.327 (11) Å is longer than the Pd–C_{62} and Pd–C_{63} lengths of 2.144 (12) and 2.101 (11) Å, respectively. Again note that there is a small but statistically significant difference between the coordination of Pd to C_{62} and C_{63}. The projection of Pd onto the C_3 ring, while lying approximately on the C_{62}–C_{63} vector, is closer to C_{63} than C_{62}.

The structure of the hexafluorophosphate salt of palladium, **3** (Figure 3c), shows remarkable stereochemical differences in comparison to that of **2**. The PdP_2 moiety has rotated by 11° from that in **2** so that it and the C_{62}–C_{63} axis form an angle of 0°. The projection of the Pd atom onto the C_3 plane no lies outside of the ring. The PdP_2 and C_3 planes are also no longer orthogonal. The dihedral angle is 105°. The bond lengths (and angles) within the C_3 unit are equal within the standard deviations to that found in **2**. The Pd–C_{61} distance has increased from that in **2** to 2.391 (9) Å. The remaining Pd–C bond lengths are equalized at 2.10 (1) Å (average).

As previously mentioned the platinium hexafluorophosphate derivative, **4**, for which structural parameters are partially available,[6] is isostructural with **3**. There are, however, significant differences. The dihedral angle between the MP_2 and C_3 planes in **4** has increased to 111°. As in **3** the dihedral angle between the C_{62}–C_{63} axis and the MP_2 plane is 0°. The C_{62}–C_{63} bond has lengthened to 1.58 (2) Å while the other two C–C bonds in the C_3 ring do not significantly change in comparison to those in **3**. The projection of the Pt atom onto the C_3 plane again lies on the bisector of the C_{62}–C_{63} bond; however, compared to **3** it lies even more outside of the C_3 ring. The distance of the projection to C_{61} in **3** is 1.38 Å; that in **4** was found to be 1.62 Å. The Pt–P bond lengths in **4** are shorter than the Pd–P lengths in **2** and **3**, presumably due to the lanthanide contraction effect.[23]

The distinctive arrangement of the phenyl groups connected to the cyclopropenium ring deserves some comment. As previously noted[13a] for cyclopropenium complexes there is a correlation between phenyl tilt angles, phenyl twist angles, and the exocyclic C–C bond lengths which connect the phenyl groups to the C_3 ring. The phenyl tilt angles are defined as arc sin (d_1/d_2) where d_1 is the distance of the first atom of the phenyl group from the C_3 ring plane and d_2 is the exocyclic bond length. The twist angle is the dihedral angle between the plane of a phenyl group and the C_3 ring plane. The tilt and twist angles are reported at the bottom of Table V. The general pattern that is observed[13a] is that the more twisted and tilted the phenyl groups are, the longer will be the exocyclic C–C distance because of the decreased conjugation between the phenyl groups and the cyclopropenium ring. The relationship holds well for the nickel complex, **1**, where the exocyclic distances, C_{61}–C_{37}, C_{62}–C_{43}, and C_{63}–C_{49}, become progressively shorter as the tilt and twist angles decrease. We also note that the closer the metal atom is to one of the carbons in the C_3 ring, the more tilted and twisted the phenyl group connected to it becomes. These relationships also hold well for the hexafluorophosphate salt of palladium, **3**, with one short and two longer exocyclic distances. However, in **2**, all three exocyclic distances are approximately the same. In fact all three distances are as short as the shortest in **1** and **3**. A discussion of the relationship between the tilt angles and the ring-whizzing will be presented later.

The Bonding and Theoretical Account of the Distortions

(Cyclopropenium)$Ni(PH_3)_2$ was chosen as the model for the calculations in this study. Before discussing the geometrical optimizations and the potential surface for ring-whizzing, we shall discuss the bonding in the complex. The important valence orbitals can be derived by interacting the orbitals of a d^{10} ML_2 fragment

(23) Cotton, F. A.; Wilkinson, G. "Advanced Inorganic Chemistry", 4th ed.; Wiley: New York, 1980; p 822.

Table III. Final Atomic Parameters for $[(PPh_3C_3)Pd(PPh_3)_2]PF_6 \cdot C_6H_6$

(a) Anisotropically Refined Atoms

atom	x	y	z	U_{11}	U_{22}	U_{33}	U_{12}	U_{13}	U_{23}
Pd	1714 (1)	−863 (1)	2966 (1)	38 (1)	36 (1)	33 (1)	2 (1)	1 (1)	2 (1)
P1	2867 (2)	−591 (1)	3934 (1)	46 (1)	45 (1)	38 (1)	−3 (1)	−2 (1)	−5 (1)
P2	1321 (2)	−33 (1)	2302 (1)	45 (1)	40 (1)	40 (1)	2 (1)	0 (1)	4 (1)
P3	4147 (3)	1831 (1)	9018 (2)	64 (2)	69 (2)	76 (2)	0 (2)	15 (2)	12 (2)

(b) Isotropically Refined Atoms

atom	x	y	z	U, Å^3	atom	x	y	z	U, Å^3
F1	3940 (12)	2394 (7)	8596 (8)	131 (6)	C24	2315 (4)	912 (3)	2895 (4)	69 (3)
F2	2865 (12)	1701 (6)	8960 (9)	132 (6)	C25	2253 (5)	73 (2)	1565 (3)	44 (2)
F3	4195 (13)	1531 (7)	8261 (9)	147 (7)	C26	2330 (5)	591 (2)	1221 (3)	61 (3)
F4	4349 (13)	1233 (7)	9351 (9)	132 (6)	C27	3034 (5)	655 (2)	648 (3)	67 (3)
F5	3986 (14)	2086 (7)	9773 (9)	147 (7)	C28	3661 (5)	203 (2)	418 (3)	72 (3)
F6	5391 (10)	1999 (5)	9038 (7)	108 (5)	C29	3584 (5)	−315 (2)	761 (3)	70 (3)
F7	4776 (21)	1543 (11)	9705 (14)	133 (11)	C30	2880 (5)	−379 (2)	1335 (3)	58 (3)
F8	4222 (23)	2444 (14)	9406 (17)	154 (13)	C31	−41 (5)	−87 (3)	1876 (3)	47 (2)
F9	3063 (23)	1804 (12)	9466 (18)	126 (11)	C32	−273 (5)	81 (3)	1172 (3)	60 (3)
F10	5210 (25)	1760 (13)	8595 (19)	153 (12)	C33	−1330 (5)	9 (3)	875 (3)	82 (4)
F11	3931 (29)	1211 (16)	8820 (22)	196 (15)	C34	−2157 (5)	−230 (3)	1282 (3)	78 (3)
F12	3484 (32)	2147 (17)	8409 (20)	179 (14)	C35	−1925 (5)	−398 (3)	1986 (3)	76 (3)
C61	551 (7)	−1672 (4)	2954 (5)	46 (2)	C36	−867 (5)	−326 (3)	2283 (3)	58 (3)
C62	1678 (7)	−1742 (3)	2969 (5)	43 (2)	C37	−470 (5)	−1796 (3)	3297 (3)	46 (2)
C63	1075 (7)	−1523 (4)	2333 (5)	43 (2)	C38	−1471 (5)	−1737 (3)	2920 (3)	61 (3)
C1	4030 (5)	−223 (3)	3557 (3)	48 (2)	C39	−2455 (5)	−1884 (3)	3243 (3)	85 (4)
C2	4437 (5)	287 (3)	3814 (3)	59 (3)	C40	−2438 (5)	−2090 (3)	3942 (3)	91 (4)
C3	5262 (5)	567 (3)	3448 (3)	76 (3)	C41	−1437 (5)	−2149 (3)	4319 (3)	86 (4)
C4	5679 (5)	335 (3)	2825 (3)	79 (3)	C42	−453 (5)	−2002 (3)	3997 (3)	66 (3)
C5	5271 (5)	−175 (3)	2567 (3)	70 (3)	C43	2563 (4)	−2132 (3)	3172 (3)	45 (2)
C6	4447 (5)	−454 (3)	2933 (3)	59 (3)	C44	2402 (4)	−2535 (3)	3699 (3)	64 (3)
C7	2314 (5)	−126 (3)	4602 (3)	46 (2)	C45	3244 (4)	−2912 (3)	3878 (3)	84 (4)
C8	1349 (5)	172 (3)	4441 (3)	73 (3)	C46	4246 (4)	−2886 (3)	3529 (3)	83 (4)
C9	925 (5)	543 (3)	4941 (3)	92 (4)	C47	4406 (4)	−2483 (3)	3001 (3)	77 (3)
C10	1466 (5)	616 (3)	5603 (3)	86 (4)	C48	3565 (4)	−2105 (3)	2822 (3)	58 (3)
C11	2431 (5)	319 (3)	5674 (3)	98 (4)	C49	1003 (4)	−1575 (3)	1549 (4)	46 (2)
C12	2854 (5)	−53 (3)	5263 (3)	78 (3)	C50	40 (4)	−1429 (3)	1169 (4)	61 (3)
C13	3512 (5)	−1129 (3)	4496 (4)	52 (3)	C51	17 (4)	−1439 (3)	421 (4)	88 (4)
C14	2827 (5)	−1476 (3)	4890 (4)	87 (4)	C52	956 (4)	−1594 (3)	54 (4)	95 (4)
C15	3284 (5)	−1889 (3)	5334 (4)	99 (4)	C53	1919 (4)	−1740 (3)	434 (4)	82 (4)
C16	4426 (5)	−1956 (3)	5385 (4)	105 (4)	C54	1942 (4)	−1730 (3)	1181 (4)	64 (3)
C17	5111 (5)	−1610 (3)	4992 (4)	111 (5)	C55	349 (7)	3287 (4)	7014 (7)	136 (6)
C18	4654 (5)	−1196 (3)	4547 (4)	82 (4)	C56	623 (7)	3591 (4)	6406 (7)	131 (6)
C19	1309 (4)	652 (3)	2733 (4)	52 (3)	C57	1711 (7)	3756 (4)	6307 (7)	133 (6)
C20	327 (4)	899 (3)	2947 (4)	72 (3)	C58	2527 (7)	3617 (4)	6817 (7)	144 (6)
C21	352 (4)	1404 (3)	3322 (4)	90 (4)	C59	2254 (7)	3313 (4)	7425 (7)	146 (6)
C22	1359 (4)	1663 (3)	3484 (4)	94 (4)	C60	1165 (7)	3148 (4)	7524 (7)	143 (6)
C23	2340 (4)	1417 (3)	3270 (4)	90 (4)					

[a] The form of the thermal ellipsoid is $\exp[-2\pi^2(U_{11}h^2a^{*2} + U_{22}k^2b^{*2} + U_{33}l^2c^{*2} + 2U_{12}hka^*b^* + 2U_{13}hla^*c^* + 2U_{23}klb^*c^*)]$. Coordinates multiplied by 10^4, temperature factors by 10^3. [b] Coordinates multiplied by 10^4, temperature factors by 10^3. The population parameter of atoms F1–F6 was refined to the value 0.63 (2); the population parameter of atoms F7–F12 was constrained to be the complement to 1 of the previous value.

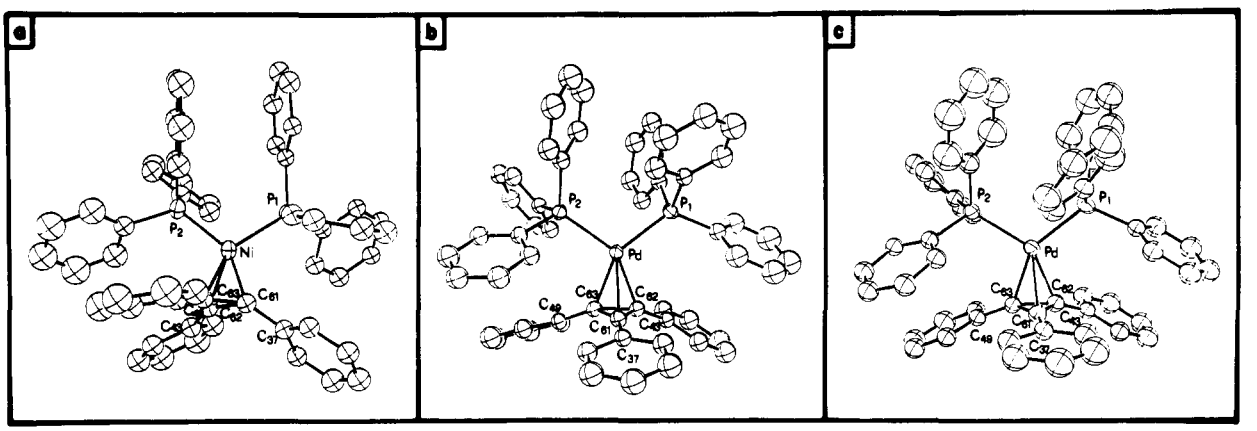

Figure 3. ORTEP drawings of the $[(Ph_3C_3)M(PPh_3)_2]^+X^-$ cations: (a) M = Ni, X = PF_6. (b) M = Pd, X = ClO_4. (c) M = Pd, X = PF_6.

with the cyclopropenium cation. This is done at the η^3 geometry with the conformation of the ML_2 groups as indicated by **8a**. As we shall see, rotation at η^3 to the alternative conformation, **8b**, leads to an essentially identical situation. The interaction diagram for **8a** is shown in Figure 4. The three π orbitals, a_2'' and e'', of the cyclopropenium cation are displayed on the right side of the figure. Notice that there are also two high-lying σ orbitals, the Walsh set (e'). These will also play a role, mainly in offering

Table IV. Final Atomic Parameters for $[(Ph_3C_3)Pd(PPh_3)_2]ClO_4$

(a) Anisotropically Refined Atoms

atom	x	y	z	U_{11}	U_{22}	U_{33}	U_{12}	U_{13}	U_{23}
Pd	1933 (1)	3629 (1)	2602 (1)	40 (1)	50 (1)	46 (1)	3 (1)	3 (1)	−3 (1)
P1	3075 (3)	3363 (3)	4275 (3)	44 (2)	66 (3)	46 (2)	10 (2)	3 (2)	−3 (2)
P2	1709 (3)	4279 (1)	2882 (3)	41 (2)	52 (2)	52 (2)	4 (2)	6 (2)	−6 (2)
Cl	219 (4)	1225 (1)	4253 (4)	56 (2)	83 (3)	94 (3)	7 (2)	10 (2)	−7 (2)

(b) Isotropically Refined Atoms

atom	x	y	z	U, Å^2	atom	x	y	z	U, Å^2
O1	1385 (20)	1161 (6)	4179 (17)	236 (9)	C30	3132 (9)	4441 (3)	4939 (10)	135 (8)
O2	242 (13)	1225 (4)	5384 (13)	155 (5)	C31	136 (8)	4438 (2)	2190 (6)	52 (3)
O3	−407 (17)	921 (6)	3754 (15)	208 (7)	C32	−849 (8)	4235 (2)	2410 (6)	60 (4)
O4	−183 (14)	1564 (5)	3760 (13)	163 (6)	C33	−2070 (8)	4327 (2)	1876 (6)	74 (4)
C61	388 (11)	3250 (3)	1530 (10)	54 (4)	C34	−2307 (8)	4623 (2)	1122 (6)	66 (4)
C62	1558 (11)	3190 (4)	1393 (10)	53 (3)	C35	−1323 (8)	4827 (2)	902 (6)	66 (4)
C63	865 (10)	3533 (3)	994 (10)	48 (3)	C36	−101 (8)	4734 (2)	1436 (6)	53 (3)
C1	2149 (8)	3397 (3)	5275 (9)	61 (4)	C37	−649 (8)	3087 (3)	1868 (8)	57 (4)
C2	2592 (8)	3318 (3)	6391 (9)	134 (7)	C38	−502 (8)	2736 (3)	2378 (8)	80 (5)
C3	1811 (8)	3359 (3)	7096 (9)	135 (8)	C39	−1474 (8)	2578 (3)	2748 (8)	114 (6)
C4	587 (8)	3478 (3)	6685 (9)	100 (6)	C40	−2593 (8)	2773 (3)	2607 (8)	114 (6)
C5	143 (8)	3557 (3)	5569 (9)	105 (6)	C41	−2740 (8)	3125 (3)	2097 (8)	102 (6)
C6	924 (8)	3516 (3)	4864 (9)	85 (5)	C42	−1768 (8)	3282 (3)	1727 (8)	78 (4)
C7	3361 (7)	2857 (2)	4238 (7)	51 (3)	C43	2406 (8)	2915 (2)	1147 (7)	51 (3)
C8	4445 (7)	2724 (2)	3999 (7)	76 (4)	C44	3452 (8)	3047 (2)	839 (7)	69 (4)
C9	4593 (7)	2339 (2)	3845 (7)	80 (5)	C45	4290 (8)	2793 (2)	578 (7)	85 (5)
C10	3657 (7)	2087 (2)	3929 (7)	82 (5)	C46	4083 (8)	2406 (2)	625 (7)	85 (5)
C11	2574 (7)	2221 (2)	4168 (7)	78 (4)	C47	3037 (8)	2274 (2)	934 (7)	85 (5)
C12	2425 (7)	2605 (2)	4323 (7)	66 (4)	C48	2199 (8)	2529 (2)	1195 (7)	66 (4)
C13	4615 (11)	3558 (3)	4846 (8)	63 (4)	C49	531 (6)	3788 (2)	68 (7)	52 (3)
C14	5247 (11)	3535 (3)	5951 (8)	115 (6)	C50	1456 (6)	3898 (2)	−441 (7)	65 (4)
C15	6386 (11)	3718 (3)	6329 (8)	121 (7)	C51	1169 (6)	4140 (2)	−1343 (7)	93 (5)
C16	6893 (11)	3923 (3)	5601 (8)	121 (7)	C52	−42 (6)	4272 (2)	−1737 (7)	86 (5)
C17	6261 (11)	3946 (3)	4496 (8)	131 (9)	C53	−967 (6)	4163 (2)	−1229 (7)	74 (4)
C18	5122 (11)	3764 (3)	4118 (8)	117 (6)	C54	−680 (6)	3921 (2)	−326 (7)	63 (4)
C19	2760 (8)	4571 (2)	2341 (7)	53 (3)					
C20	3414 (8)	4398 (2)	1660 (7)	59 (4)					
C21	4221 (8)	4610 (2)	1210 (7)	85 (5)					
C22	4375 (8)	4994 (2)	1439 (7)	85 (5)					
C23	3721 (8)	5167 (2)	2120 (7)	79 (4)					
C24	2914 (8)	4955 (2)	2571 (7)	73 (4)					
C25	1919 (9)	4456 (3)	4284 (10)	67 (4)					
C26	956 (9)	4579 (3)	4728 (10)	131 (7)					
C27	1207 (9)	4687 (3)	5827 (10)	136 (8)					
C28	2420 (9)	4672 (3)	6483 (10)	130 (7)					
C29	3383 (9)	4549 (3)	6039 (10)	132 (9)					

[a] The form of the themal ellipsoid is $\exp[-2\pi^2(U_{11}h^2a^{*2} + U_{22}k^2b^{*2} + U_{33}l^2c^{*2} + 2U_{12}hka^*b^* + 2U_{13}hla^*c^* + 2U_{23}klb^*c^*)]$. Coordinates multiplied by 10^4, temperature factors by 10^3. [b] Coordinates multiplied by 10^4, temperature factors by 10^5.

8a **8b**

a set of repulsive interactions. The orbitals of a d^{10} ML_2 fragment, displayed on the left side of Figure 4, have been extensively discussed elsewhere.[15,19,24] At low energy are four closely spaced levels, $b_2 + 1a_1 + a_2 + 2a_1$, which are readily identifiable with the $e_g + b_{2g} + a_{1g}$ set of a traditional square-planar ML_4 system. At higher energy is b_1. This orbital is hybridized[19] out away from the L groups toward the cyclopropenium side. At much higher energy is $3a_1$, a cylindrically symmetric orbital again hybridized away from the L groups. The b_1 orbital is the highest occupied molecular orbital (HOMO) of a d^{10} ML_2 fragment, and the $3a_1$ is the lowest unoccupied molecular orbital (LUMO). At much higher energy than $3a_1$ is an essentially pure metal p orbital of b_2 symmetry (not shown in this figure). When the two fragments are interacted in **8a**, a multitude of mixings occurs since the symmetry of **8a** is only C_s. We present only the salient details. Orbitals a_2'', $1a_1$, and $3a_1$ form three combinations. The two at lower energy, 1a′ and 3a′, in the middle of Figure 4 are filled. The a_2 and $2a_1$ orbitals of ML_2 are slightly destabilized by the cyclopropenium e′ set giving 2a″ and 5a′, respectively. The e′ and e″ levels combine strongly with b_1 and b_2 of ML_2. Molecular orbitals 2a′ and 1a″ are the bonding combination of b_2 and b_1, respectively, with e′. The 4a′ and 3a″ levels are primarily centered on b_2 and b_1, respectively. In these two molecular orbitals, b_2 and b_1 are bonding with respect to e″ and antibonding with respect to e′. To simplify the situation we could ignore the σ-centered e′ levels of the cyclopropenium unit. Orbitals 3a″ and 4a′ can be represented by **9a** and **9b**, respectively. Together with the

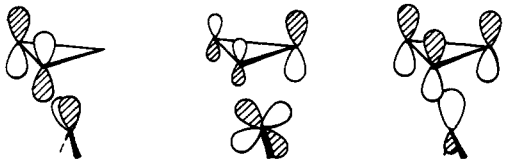

9a **9b** **9c**

interaction between $3a_1$ of ML_2 and a_2'', **9c**, these are the dominant bonding factors which hold the ML_2 unit to the cyclopropenium ring. The consequence of e′ involvement is to provide a set of repulsions which can be partially removed by distortion.

Before describing potential distortions, one important detail

(24) (a) Burdett, J. K. *Inorg. Chem.* **1975**, *14*, 375; *J. Chem. Soc., Faraday Trans. II* **1974**, *70*, 1599. (b) Hofmann, P. *Angew. Chem.* **1977**, *89*, 551; Habilitation, University of Erlangen, 1978.

Table V. Selected Bond Lengths (Å) and Angles (deg)

	$[(Ph_3C_3)Ni(PPh_3)_2]PF_6$	$[(Ph_3C_3)Pd(PPh_3)_2]PF_6 \cdot C_6H_6$	$[(Ph_3C_3)Pd(PPh_3)_2]ClO_4$
M-P1	2.241 (4)	2.349 (3)	2.365 (3)
M-P2	2.234 (4)	2.378 (3)	2.358 (3)
M-C61	1.897 (12)	2.391 (9)	2.327 (11)
M-C62	2.009 (12)	2.097 (8)	2.144 (12)
M-C63	2.056 (10)	2.106 (9)	2.101 (11)
C61-C62	1.445 (18)	1.376 (12)	1.371 (18)
C61-C63	1.425 (20)	1.382 (13)	1.387 (18)
C62-C63	1.329 (21)	1.474 (13)	1.461 (16)
C61-C37	1.480 (17)	1.440 (11)	1.444 (17)
C62-C43	1.473 (18)	1.463 (10)	1.443 (16)
C63-C49	1.452 (18)	1.470 (11)	1.450 (16)
P1-C1	1.839 (8)	1.818 (7)	1.819 (12)
P1-C7	1.825 (10)	1.809 (7)	1.825 (9)
P1-C13	1.829 (9)	1.823 (8)	1.820 (11)
P2-C19	1.828 (12)	1.823 (8)	1.816 (9)
P2-C25	1.811 (10)	1.821 (7)	1.831 (13)
P3-C31	1.820 (11)	1.821 (6)	1.836 (8)
P1-M-P2	107.3 (1)	106.1 (1)	108.1 (1)
P1-M-C61	107.2 (4)	124.8 (2)	116.1 (3)
P1-M-C62	140.7 (4)	106.7 (3)	107.9 (3)
P1-M-C63	134.8 (4)	147.4 (3)	147.2 (3)
P2-M-C61	149.7 (4)	123.9 (2)	124.2 (3)
P2-M-C62	109.4 (4)	146.1 (3)	143.9 (3)
P2-M-C63	109.8 (4)	105.4 (3)	104.3 (3)
C61-M-C62	43.3 (5)	34.9 (3)	35.4 (5)
C61-M-C63	42.0 (6)	35.1 (3)	36.1 (5)
C62-M-C63	38.2 (6)	41.1 (3)	40.2 (4)
C62-C61-C63	55.2 (9)	64.6 (6)	64.0 (9)
C61-C62-C63	61.6 (1.0)	57.9 (6)	58.6 (9)
C61-C63-C62	63.2 (1.0)	57.5 (6)	57.5 (9)
M-C61-C62	77.5 (7)	60.8 (5)	65.0 (7)
M-C61-C63	74.9 (7)	61.1 (5)	63.1 (6)
M-C62-C61	64.2 (7)	84.3 (5)	79.6 (8)
M-C62-C63	72.8 (8)	69.8 (5)	68.3 (6)
M-C63-C61	63.0 (6)	83.8 (6)	80.9 (7)
M-C63-C62	69.0 (6)	69.2 (5)	71.4 (6)
M-C61-C37	142.6 (8)	132.5 (6)	126.0 (8)
C62-C61-C37	133.6 (1.3)	146.2 (8)	145.7 (1.1)
C63-C61-C37	139.6 (9)	147.7 (8)	149.6 (1.1)
M-C62-C43	130.5 (7)	128.4 (6)	128.4 (7)
C61-C62-C43	145.7 (1.2)	143.5 (8)	145.5 (1.1)
C63-C62-C43	145.9 (1.2)	141.2 (8)	143.7 (1.2)
M-C63-C49	129.0 (9)	129.3 (6)	130.0 (7)
C61-C63-C49	143.0 (1.1)	142.8 (8)	142.3 (1.0)
C62-C63-C49	150.3 (1.2)	142.1 (8)	143.5 (1.2)
Tilt Angles of Phenyl Groups (deg)[a]			
C61-C37	34.6	7.4	4.9
C62-C43	15.6	25.2	21.8
C63-C49	11.1	25.3	24.5
Twist Angles of Phenyl Groups (deg)[a]			
C61-C32	36.6	11.6	3.0
C62-C43	26.4	29.7	27.6
C63-C49	11.2	23.6	25.9

[a] Defined in the text and in ref 13a.

remains. Which of the three bonding interactions, **9a–c**, is the largest? The answer is found by the usual[25] analysis in perturbation theory. That combination having the smallest energy gap between fragment orbitals and the largest overlap will have the largest interaction. Although the overlap is large, the energy gap between $3a_1$ and a_2'' is quite large. The b_1 fragment orbital lies higher in energy than b_2 and, hence, closer to e″. Furthermore, b_1 is hybridized toward the cyclopropenium ring and will have a large overlap with one component of e″; b_2 is not hybridized. The calculated group overlaps[26] are shown in Figure 5. The vertical line toward the middle of this figure serves as a reference point to the η^3 geometry. The larger overlap of b_1 with e″ compared to b_2 is clearly displayed. In summary, the largest interaction between a d^{10} ML_2 and a cyclopropenium cation is contained within **9a**.

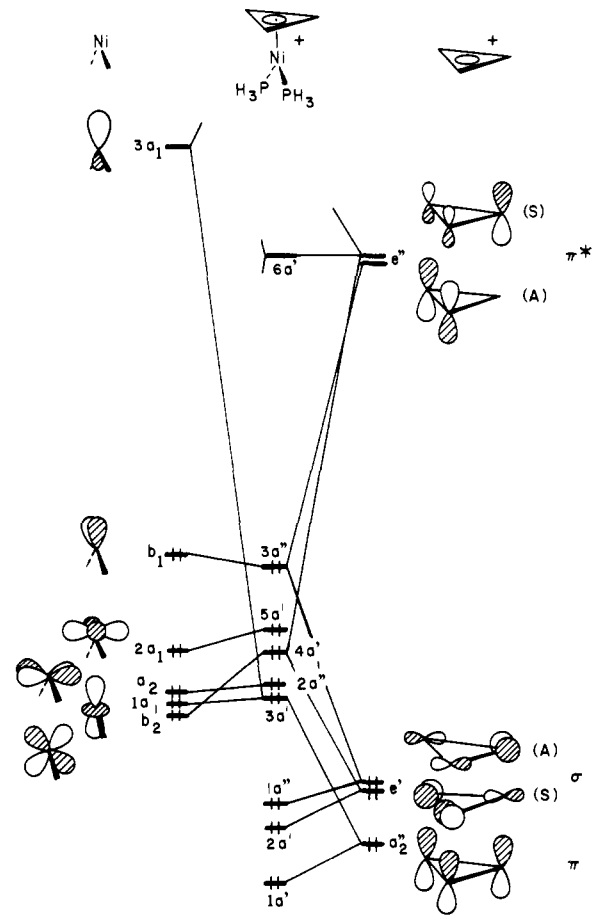

Figure 4. Orbital interaction diagram for (cyclopropenium)ML_2^+ at the η^3 geometry.

Let us now allow the molecule to relax by shifting toward a carbon–carbon bond, in other words, toward an η^2 structure, **10**.

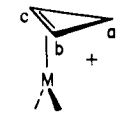

10

This could be done in a variety of ways. The most thorough method would be to optimize the Ni to C_3 plane distance independently along with the slipping motion. Given the unreliability of the extended Hückel method to optimize bond lengths correctly, we have done this in a way so that the Ni–C_b and Ni–C_c (see **10**) distances were held constant. This is found to be a stabilizing distortion for two reasons. First of all, slipping to **10** increases the interaction between b_1 and the antisymmetric combination of e″ (e″$_{(A)}$ shown in **9a**). The modest increase in overlap between the fragment orbitals is plotted to the left of Figure 5. Secondly, much of the repulsive interactions between ML_2 and e′ is lost. Counteracting this tendency is that the overlap between b_2 and the symmetric component of e″ (e″$_{(S)}$, shown in **9b**) along with $3a_1$ and a_2'', **9c**, is diminished. This is also indicated on the left side of Figure 5. There is one further point. When the ML_2 is at η^2 and beyond the periphery of the ring, an interaction between $3a_1$ and e′$_{(s)}$ is turned on. This, along with the b_1 + e″$_{(A)}$ combination, evolves into symmetry-adapted linear combinations of the two metal–carbon σ orbitals for the product of oxidative addition, **11**. The reaction **10** to **11** is symmetry allowed.[14] Later

11

(25) Hoffmann, R. *Acc. Chem. Res.* **1971**, *4*, 1.
(26) The fragment orbital analysis has been developed in: Hoffmann, R.; Swenson, J. R.; Wan, C.-C. *J. Am. Chem. Soc.* **1973**, *95*, 7644. Fujimoto, H.; Hoffmann, R. *J. Phys. Chem.* **1974**, *78*, 1167.

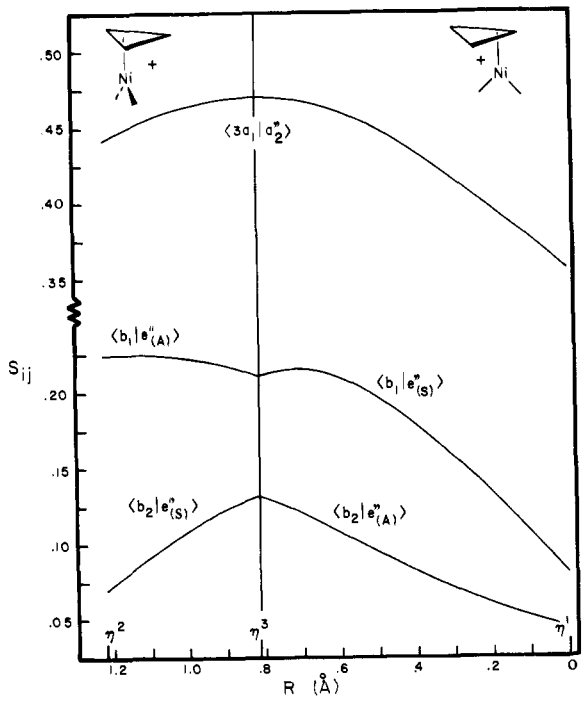

Figure 5. Values of the overlap between fragment orbitals for slipping the $Ni(PH_3)_2$ group away from η^3 for the conformations indicated at the top of the figure. R is defined in **12** and **22**.

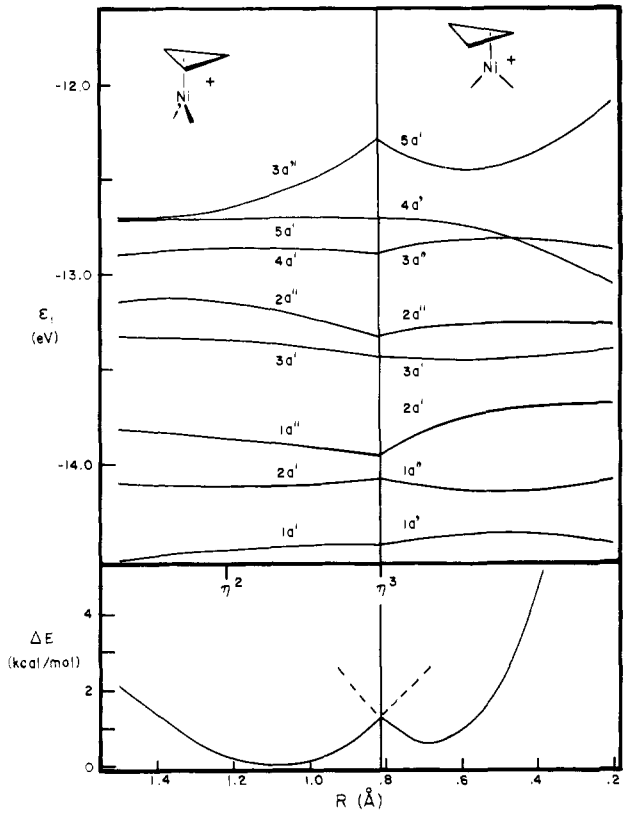

Figure 6. At the top the orbital energies (eV) are plotted for slipping the $Ni(PH_3)_2$ group away from η^3 in the conformations indicated. The bottom of this figure shows the variation of the relative total energy (kcal/mol). R is defined in **12** and **22**.

we present strategies for pushing the system toward **11**.

A plot of the orbital energies along with the total energy is displayed on the left side of Figure 6. R in this figure as well as in Figure 5 is taken to be the distance of the projection of the metal atom onto the plane of the cyclopropenium ring to the unique carbon, C_a. The optimum value for R was found to be at 1.06 Å (a "pure" η^2 geometry would be at 1.221 Å, and η^3 lies at 0.814 Å). One can see that the HOMO, 3a'', falls to lower energy and then is relatively constant at distances well outside of the cyclopropenium triangle. The total energy also reflects this as seen at the bottom left of Figure 6. The agreement between the structural results and theory can be made much better for an η^2-like structure by allowing further geometrical deformations to occur.

Next, the tilting angles, τ_2, defined in **12**, were allowed to vary along with θ, the dihedral angle between the $Ni(PH_3)_2$ and cyclopropenium planes, and R. For convenience τ_1 was held constant at 0°. The optimum structure now was one where R = 1.05 Å, θ = 107°, and τ_2 = 25°. This corresponds to a distance for the projection of the Ni atom onto the plane of the cyclopropenium frame to C_a of 1.39 Å. In the Pt structure this value is 1.6 Å (R = 0.97 Å, θ = 111°). Our calculations put this to be at only 0.3 kcal/mol higher energy than the optimized structure. This point lies to the left (away from η^2) of our calculated minimum. The $Pd^+PF_6^-$ structure, **3**, is calculated to lie at a point 0.2 kcal/mol less stable on the right side of the minimum. The value of τ_2 in **3** was 25° (τ_1 = 7°), identical with our computed value. This highlights the fact that very minor changes in nonbonded contacts can cause substantial changes in the structure. In other words, the potential surface is very flat in this region, particularly away from η^2 towards the oxidative addition product.

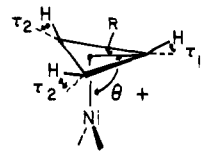

12

A rationalization of why θ and τ_2 increase from 90° and 0°, respectively, lies again in the b_1–$e''_{(A)}$ interaction, redrawn somewhere near η^2 in **13**. As previously discussed, $e'_{(A)}$ mixes into **13** in an antibonding way, **14**. This reorients the cyclopropenium component to that in **15a**. Increasing θ, as in **15b**, will stengthen the overlap with b_1. Increasing τ_2 serves to hybridize the lobes on C_b and C_c toward the ML_2 unit, just as pinning back the hydrogens does in d^{10} ML_2 complexes of olefins.[19]

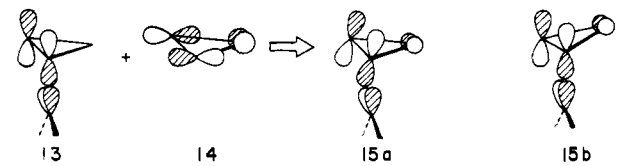

13 **14** **15a** **15b**

One last geometrical detail is noteworthy in the η^2 structure, the C_a–C_b and C_b–C_c bond lengths. As noted previously, the extended Hückel method is unreliable for the calculation of bond lengths, so we have not tried to include this in our optimization. However, the calculated C–C overlap populations at η^2 (R = 1.221 Å, θ = 90°) were 0.909 and 0.829 for C_a–C_b and C_b–C_c, respectively. This predicts that the C_a–C_b (and C_a–C_c) bond should be shorter than C_b–C_c, which is in agreement with the structural results of **3** and **4**. The reason behind this lies in the b_2–b_1 difference. In a formal way, consider b_2 and b_1 to be filled and e'' empty before Interaction. When the interaction is turned on, charge drifts from b_2 and b_1 to e''. The amount is governed by the strength of the interaction. We calculate that 0.37 electron is transferred to $e''_{(A)}$, shown by a top view in **16**, and 0.09 electron

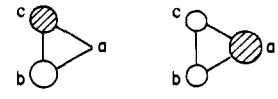

16 **17**

to $e''_{(S)}$, **17**, at η^2 (R = 1.221 Å, θ = 90°). There is a node between C_b and C_c in $e''_{(A)}$ which, therefore, diminishes the C_b–C_c overlap population.

A corollary is that, on moving from η^3 to η^2 and beyond the

perimeter of the ring, the overlap between b_1 and $e''_{(A)}$ rises to a maximum and stays relatively constant. That between b_2 and $e''_{(s)}$ steadily falls (see Figure 5). Therefore the occupation of $e''_{(A)}$ should increase, and $e''_{(s)}$ should lessen moving along the distortion. Consequently, the C_b–C_c, C_a–C_b (C_a–C_c) bond length differential becomes larger. This is precisely what occurs when a comparison is made of the structural results in **3** and **4**.

Let us return now to η^3 and rotate the ML_2 by 90° to **8b**. The total energy calculated for **8a** and **8b** is essentially the same. In **8b**, b_1 is now symmetric with respect to the mirror plane and, therefore, it interacts with $e''_{(s)}$ and $e'_{(s)}$. Orbital b_2 is antisymmetric and will combine with $e''_{(A)}$ and $e'_{(A)}$. The dominant bonding interactions are now **18**–**20**. As can be seen from Figure

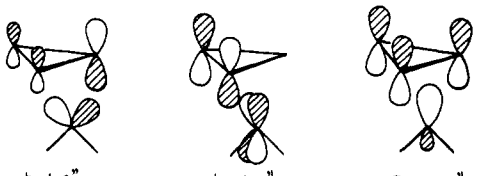

18 **19** **20**

5, the group overlaps are the same. Orbital $3a_1$ is cylindrically symmetric so its overlap with a_2'' is identical no matter what the conformation of the ML_2 unit is in the molecule. Orbitals $e''_{(s)}$ and $e''_{(A)}$ are degenerate. At η^3 the overlap of each with b_1 must be identical. The principal interaction is **18**. If ML_2 were to slip to η^2, the overlap between b_1 and $e''_{(s)}$ becomes smaller. Although the b_2–$e''_{(A)}$ overlap becomes larger, the dominance of the former interaction causes a net destabilization indicated by the dashed line to the left of η^3 at the bottom of Figure 6. If the slippage is in the opposite direction, toward η^1, a stabilization ensues.

The reason is traced by group overlaps in the right of Figure 5 and orbital energies on the right side of Figure 6. Here again we have slipped the ML_2 unit in such a way so that the Ni–C_a distance, **21**, remains constant. In this motion the calculated

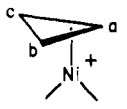

21

overlap between b_1 and $e''_{(s)}$ actually increases a bit from η^3 and then drops. The b_2–$e''_{(A)}$ and $3a_1$–a_2'' overlaps uniformly decrease. The HOMO, now 5a′ in Figure 6, drops in energy from movement away from η^3 and then rises as ML_2 becomes close to η^1. Orbital 5a′ is principally $b_1 + e''_{(s)}$, **18**, with $e'_{(s)}$ mixed in antibonding with respect to b_1. The energetic variations of the other orbitals can be developed along similar lines. The main driving force for the distortion is the increased overlap between b_1 and $e''_{(s)}$ and diminished repulsive interactions with e′. If the ML_2 group were rotated by 90° back to **8a** and the distortion to η^1 took place, we calculate that the total energy, relative to η^3, rises. This is indicated by the dashed line to the right of η^3 at the bottom of Figure 6. The argument is a simple variant to that given previously for slipping **8b** to η^2. The overlap between b_1 and $e''_{(A)}$ diminishes.

Further geometrical optimizations were carried out on **21**. Now the two independent values of τ, R, and θ, defined again by **22**,

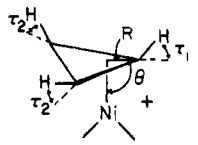

22

were varied. We find that the optimum structure is one where $R = 0.64$ Å, $\theta = 90°$, $\tau_1 = 21°$, and $\tau_2 = 8°$. It is 2.9 kcal/mol less stable than the optimized value for η^2. We will call this geometry the "crossover structure" for reasons that will become apparent. An η^3 structure where $R = 0.814$ Å was found to have optimum values of $\theta = 90°$, $\tau_1 = 17°$, $\tau_2 = 11°$ with a total energy 4.5 kcal/mol less stable than η^2 (1.6 kcal/mol less stable than the crossover structure). The structure of the Ni complex, **1**, is quite close, but not quite at the crossover structure. Experimentally, $R = 0.60$ Å, $\theta = 88°$, $\tau_1 = 35°$, and $\tau_2 = 11°$ and 16°. The larger values for τ in **1** may be a reflection of the steric bulk of the phenyl groups. Recall that in our calculations the phenyl groups have all been replaced by hydrogens. The tilting again serves to hybridize and reorient $e''_{(s)}$ towards b_1 of the ML_2 fragment. Now $e''_{(s)}$ accepts more electron density than $e''_{(A)}$ 0.39 vs. 0.14 electron. At the crossover structure the C_a–C_b (C_a–C_c) bond is expected to be longer than C_b–C_c since $e''_{(s)}$, **17**, contains a node between C_a and C_b (C_c). Our calculations put the C_a–C_b and C_b–C_c overlap populations at 0.860 and 0.919, respectively, in agreement with this. Notice that this mimics the trends in the Ni complex, **1**, where the C_{61}–C_{62} and C_{61}–C_{63} bonds are longer than C_{62}–C_{63}.

The Surface for Ring-Whizzing

We are now in a position to describe the full energy surface. Let us first review the three calculated structures for (cyclopropenium)$Ni(PH_3)_2^+$. The structures are redrawn in a view from the bottom of the complex projected onto the plane of the cyclopropenium unit in **23**–**25**. The series of molecular orbital

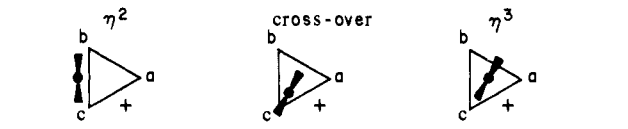

23 **24** **25**

calculations have shown that the geometrical distortions originate from the b_1–b_2 differences of ML_2 (see Figure 4). The hybridization in b_1 and its higher energy makes it a stronger bonding partner than b_2 is to the cyclopropenium π orbitals of e″ symmetry. When the ML_2 group is oriented so that it lies parallel to a C–C bond in the cyclopropenium ring (**8a**), then b_1 interacts with $e''_{(A)}$. The $b_1 + e''_{(A)}$ interaction is stabilized by slipping the ML_2 group over the C–C bond—the η^2 structure, **23**. Rotation of the ML_2 group so that it bisects a C–C (**86**) causes b_1 to interact with $e''_{(s)}$. Here again the overlap between b_1 and $e''_{(s)}$ is increased upon distortion away from the central η^3 point to the crossover structure, **24**. Besides the stereochemical activity of the b_1 orbital, repulsions from the cyclopropenium Walsh e′ set favor distortions away from η^3.

The ground-state structure which we have called η^2, **23**, corresponds to **5a–c** in Chart I. The crossover structure, **24**, is **7a–c**, and η^3, **25**, is **6** in this chart. We predict a relatively small energy difference between **23** and **24**. The ^{13}C spectra of the $[(Ph_3C_3)Pd(PPh_3)_2]PF_6$ complex are also consistent with a low barrier for ring-whizzing. A single, sharp triplet ($^2J_{^{13}C-^{31}P} = 9.2$ Hz) for the cyclopropenyl ring carbons was observed both at 20 and −90 °C. This implies that ΔG^* for the rearrangement is much less than 10 kcal/mol. In **23**–**25** the position of the cyclopropenium ring has been held constant, and, therefore, the labeling of the carbon atoms is different than that in **21**. Also notice that if θ was equal to 90° for the experimental and theoretical structures, then a description of where the ML_2 unit was in space with respect to the cyclopropenium ring would be easy. However, θ is not 90°. Rather than keeping a strict definition of this by R and θ in **12** and **22**, we shall rely on the place where the projection of the metal on the ring plane falls as a more simple descriptor. The ring-whizzing of an ML_2 unit over the face of a cyclopropenium cation is expected to occur via the crossover structure. The η^3 structure[27] does not serve as a transition state, being destabilized by 1.6 kcal/mol over the crossover structure. This is exactly what would be expected according to the McIver–Stanton theorem as discussed in the introduction. The crossover structure is less stable than

(27) We parenthetically note that with variation of the τ's there still is free rotation of the ML_2 group at η^3; i.e., structure **25** with the ML_2 group rotated by 30° is essentially energetically equivalent to **25**. The τ_1 and τ_2 values have changed; both are close to 13°.

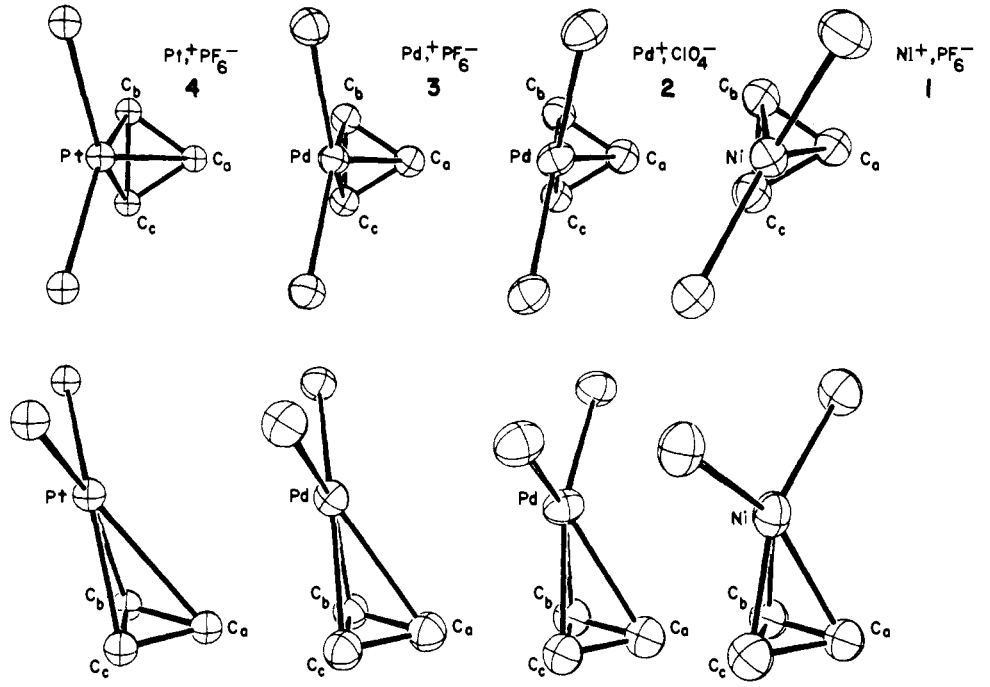

Figure 7. Top and side skeletal views of all $[(Ph_3C_3)M(PPh_3)_2]^+$ complexes. The plots were taken to be isooriented with respect to the cyclopropenium unit. The plots for Pt^+ and PF_6^- were reconstructed from the data in ref 6. In this figure C_a, C_b, and C_c correspond to C_{61}, C_{62}, and C_{63}, respectively, for the palladium compounds in Figure 3; however, they correspond to C_{63}, C_{62}, and C_{61} for the nickel complex.

η^2 for two reasons. The ML_2 group in the crossover structure is located within the triangle, close to η^3, and the repulsions between e′ and the ML_2 orbitals are more severe than in η^2. Also the overlap of b_1 with $e''_{(A)}$ at η^2 is slightly larger than that attainable between b_1 and $e''_{(S)}$ at the crossover structure. Counterbalancing this is that the overlap of 3a′ with a_2'' and b_2 with $e''_{(S)}$ or $e''_{(A)}$ is maximized at η^3 (see Figure 5).

To calculate a full surface for ring-whizzing we would need to optimize two distances, r_1 and r_2, shown in **26**, which define

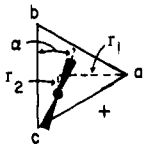

26

the position of the metal relative to the cyclopropenium ring and an ML_2 rotation angle, α, taken to be in **26** as the dihedral angle between the ML_2 plane and the C_b–C_c bond. For example, at one crossover structure r_1 = 0.90 Å, r_2 = 0.15 Å, and α = 30°. At one η^2 r_1 = 1.39 Å, r_2 = 0.0 Å, and α = 0°. The problem is that the τ's and θ defined in **12** or **22** are also strongly coupled. An exploration of the surface would require all three values of τ to be varied independently. That would mean a variation of six independent variables. A complete job would also include variation of the three C–C bond lengths and the distance of the metal to the cyclopropenium ring.[28,29] We have chosen an expedient method which fixes all τ values at 15°, θ at 90°, and the Ni to ring distance at 1.717 Å. A surface for the optimization of r_1, r_2 and α is presented in **27**. The energy contours are listed in kcal/mol. The values of r_1 and r_2 are indicated by the distance scale to the bottom and left of **27**. The distance interval was 0.1

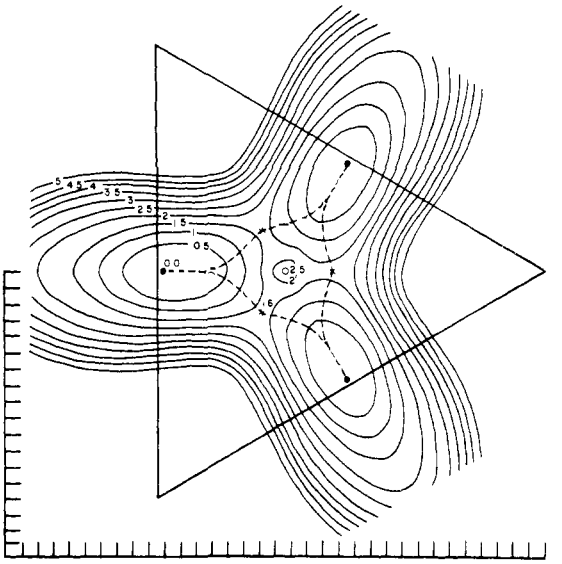

27

Å. At each point an optimum value of α was found. For easy reference the cyclopropenium ring has been inscribed on the surface. The three solid circles represent the ground states, the crosses are the transition states which interconvert η^2 geometries,

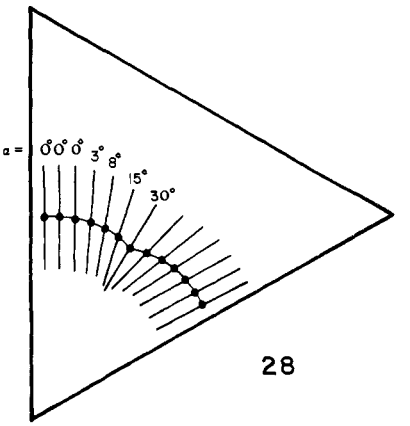

28

(28) For the optimizations of the η^2, η^3, and crossover structures, r_2 was fixed at 0.0 Å. It was then easy to devise a method for keeping the Ni–C_b and Ni–C_c or Ni–C_a distance constant depending upon which side of η^3 we were on. This is lost for any intermediate point between η^2 and the crossover structure.

(29) There are a multitude of methods for optimizing structures in an efficient manner. However, in charting a potential surface, a reaction path always needs to be defined a priori. The problem here is that the reaction path is not so easily defined. For a full discussion of this problem, see: Müller, K. *Angew. Chem.* **1980**, *92*, 1.

Table VI. Relevant Geometrical Parameters for the Ring-Whizzing Motion

	complex			
	$Pt^+PF_6^-$, 4[a]	$Pd^+PF_6^-$, 3	$Pd^+ClO_4^-$, 2	$Ni^+PF_6^-$, 1
r_1,[b] Å	1.62	1.38	1.21	1.03
r_2, Å	0.00	0.00	0.06	0.08
θ,[b] deg	111	105	89	88
α,[b] deg	0	0	11	25
C_b–C_c, Å	1.58 (2)	1.47 (1)	1.46 (2)	1.45 (2)
C_a–C_b, Å	1.40 (2)	1.38 (1)	1.37 (2)	1.33 (2)
C_a–C_c, Å	1.38 (2)	1.38 (1)	1.39 (1)	1.43 (2)
τ_a, deg	c	7	5	11
τ_b, deg	c	25	22	16
τ_c, deg	c	25	25	35

[a] Values obtained from ref 6. [b] r_1 and r_2 represent the projection of the metal onto the cyclopropenium ring distances from C_a defined in 26. α is the MP_2 rotation angle defined in 26. θ is the MP_2 tilting angle with respect to the ring and the τ values correspond to the phenyl tilting angles; both are defined in 12 or 22. Finally the cyclopropneium atom labeling scheme corresponds to that in Figure 7. [c] The value is unavailable.

and the open circle in the middle is η^3. The dashed line is the computed reaction path. It is important to realize that by fixing θ at 90° we have destabilized the ground state relative to η^3 and the crossover structure and shifted the minium to inside the ring. The fully optimized structures (**23**–**25**) more accurately display these points. The essential difference is that allowing θ at η^2 to vary shifts the projection of the Ni on the cyclopropenium plane to ~0.2 Å *outside* of the triangle. A diagram showing the optimum value of α at uniform points along the reaction path is shown in **28**. The values of α uniformly change from 0° to 30° along the reaction path from η^2 to the crossover structure.

Where do structures **1**–**4** lie with respect to this surface? Figure 7 presents a top and side view of the four structures. Table VI recasts some of the geometrical variables for **1**–**4** in terms of parameters defined in **12**, **22**, and **26** which are more appropriate for a description of the ring-whizzing motion. The twisting of the ML_2 group at the top of Figure 7 is obvious on going from **3** to **2** to **1**. **28** mimics this. As the ML_2 moves toward the interior of the ring, α increases from 0° (for **3** and **4**) up to 25° for **1**. The $Ni^+PF_6^-$ structure, **1**, is then not quite at the crossover structure. Careful inspection of the top view for **1** in Figure 7 shows that the NiP_2 unit is slightly displaced toward C_b relative to C_a. The Ni–C_{62}, Ni–C_{63} distances discussed previously also indicate this. r_1 and r_2 for the compolex were found to be 1.03 and 0.08 Å, respectively. Recall that our calculated values for the crossover structure were r_1 = 0.90 Å, r_2 = 0.15 Å, and α = 30°. It is evident from especially the side views of **4**, **3**, and **2** at the bottom left of Figure 7 that the ML_2 ring-whizzing is preceded by a "cocking" motion. The ML_2 group becomes more upright—θ decreases from 111° in **4** to 105° in **3**. This causes a decrease in the overlap between b_1 and $e''_{(A)}$. Therefore, the C_b–C_c bond length decreases and probably τ_b and τ_c also slightly decrease. Unfortunately the τ values for **4** are unavailable so we could not check this point. By the time θ has reached 90° (in **2**) the ML_2 group has started to slip and rotate. As the ML_2 unit slips across the ring there should be a breathing motion of the cyclopropenium ring. C_b–C_c and C_a–C_b should become shorter while C_a–C_c lengthens. Furthermore, τ_b should decrease greatly while τ_a and τ_c increase to a smaller extent. These predictions come from an extrapolation of what we know about the η^2 and crossover structures. The values of the C–C bond lengths and phenyl tilt angles, τ, in Table VI are partially in agreement with this. Notice that τ_a in **2** actually decreases slightly from **3** before increasing in **1** and τ_c in **3** and **2** are identical before the increase in **1**. Likewise, the relative inaccuracy in the C–C bond lengths makes a comparison of **3** and **2** tenuous.

Therefore, there seem to be two distinct phases to the ring-whizzing: the cocking motion and an actual slippage. One can thick of the reverse of the cocking motion to be oxidative insertion of the ML_2 group into a C–C bond, ultimately giving **11**. As we have previously indicated, our calculated minimum lies between the structural results of **3** and **4**, a little closer to **3**. So perhaps **4** is on the way to oxidative insertion rather than an end point for ring-whizzing—the "η^2 geometry". There is one piece of indirect evidence for this as Jemmis and Hoffman have indicated previously.[14] One might consider the η^2 structure to be a d^{10} (ethylene)ML_2 complex with a carbenium ion connected to the two ethylene carbons as in **5a**–**c**. The average C–C bond length for ethylene complexes is 1.45 Å,[30] close to that in **3** but considerably shorter than that in **4**. As we have pointed out before, the portion of the potential surface where **4** and **3** lie is calculated to be extremely flat, with full geometrical optimization. Therefore, we feel that only a statistical analysis of more structures maintaining an α value of 0° might produce a clustering of several toward a definite region in space and define the ground state.

It is tempting to attribute the positions of four structures to the identity of the metal atom. The platinum structure is at the η^2 extreme, and the nickel complex is at the other extreme, the crossover structure, with the palladium compounds intermediate. The orbitals displayed on the left side of Figure 4 are more diffuse for Pt than those of Ni. Therefore, repulsions from the cyclopropenium e′ and especially $2a_1$ and a_2 of ML_2 are expected to be larger for Pt compared to Ni. Thus, a geometry where the ML_2 group has slipped outside the ring might be anticipated. Diffuse orbitals will also abate somewhat the loss of overlap between b_2 and $e''_{(s)}$ along with $3a_1$ and a_2'' as the ML_2 unit is slipped toward η^2 (see the left side of Figure 5). But the very low potential on going from η^2 to the crossover structure makes these arguments tenuous. In the next section a different electronic way to control the solid-state structures is given.

Conclusions and Extensions

The four structures displayed in Figure 7 do remarkably well in defining the ring-whizzing motion. **3** and **4** lie close to the ground state, **1** lies close to the transition state, and **2** lies somewhere between. Because of the strong coupling of many geometrical parameters and with the accuracy and number of structures, we cannot at this time present an analytical description of the reaction path. However, the gross details of the cocking motion and the ML_2 movement and twisting are clear. One way to stabilize the crossover structure would be the substitution of an electron-withdrawing group in the ortho and/or para positions of Ar_1 in **29**. This causes the energy of $e''_{(s)}$ (see Figure 4) to drop relative to $e''_{(A)}$. Therefore, its interaction with b_1 becomes stronger.

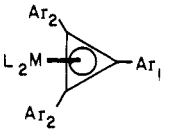

29

Alternatively, electron donors at the ortho and/or para positions of Ar_2 raise the energy of $e''_{(A)}$. This also serves to stabilize the crossover structure. The reverse substitution, electron donors at Ar_1 or acceptors at Ar_2, makes the η^2 structure more favorable. It may be possible that the ML_2 group can be pushed toward the oxidative insertion product. We shall explore these possibilities in the future. Calculations on (cyclopropenium)$Ni(CO)_2^+$ were also carried out. The η^2 structure was again found to be the ground state with the crossover structure and η^3 destabilized by 5.7 and 6.3 kcal/mol, respectively.[31] The minimum has deepened a bit from the phosphine complex, but the geometrical values for the three structures are not significantly different from those which we have presented. There are a number of (cyclopropenium)NiLX complexes known[32] where L = CO, PR_3 and X = Cl, Br. We

(30) (a) For a review of these structures, see: Ittel, S. D.; Ibers, J. A. *Adv. Organomet. Chem.* **1976**, *14*, 33. A recent listing of all structures may be found in ref 19. (b) There actually are three structures with a C–C bond length in the region of 1.50–1.53 Å. A structure of C_2Cl_4–$Pt(PPh_3)_2$ had a C–C length of 1.62 (3) Å. See: Francis, J. N.; McAdam, A.; Ibers, J. A. *J. Organomet. Chem.* **1971**, *29*, 131. The shortest C–C bond is 1.30 (2) Å for this type of complex. See Jagner, S.; Hazell, R. G.; Rasmussen, S. E. *J. Chem. Soc., Dalton Trans.* **1976**, *337*. The other values are clustered around 1.40 to 1.47 Å.

(31) The values reported here are different than those in ref 3a because more extensive geometrical optimizations were carried out.

think that these complexes are also definitely not η^3, and extended Hückel calculations bear this out, again favoring an η^2 structure.[33]

Acknowledgment. We thank F. Cecconi for technical assistance, G. Vignozzi and F. Nuzzi for microanalyses, and Professors Roald Hoffmann, Peter Lillya, and Paul Dobosh for helpful discussions. T.A.A. and J.S. thank the Robert A. Welch Foundation for generous support and the Ecole Superieure de Chimie Industrielle de Lyon for a stipend to J.S.

Registry No. $[(Ph_3C_3)Ni(PPh_3)_2]PF_6$, 75507-34-5; $[(Ph_3C_3)Pd(PPh_3)_2]ClO_4$, 79839-96-6; $[(Ph_3C_3)Pd(PPh_3)_2]PF_6 \cdot C_6H_6$, 79855-23-5; $[(Ph_3C_3)Ni(PPh_3)_2]ClO_4$, 77598-41-5; $(C_2H_4)Ni(PPh_3)_2$, 23777-40-4; $(C_2H_4)Pd(PPh_3)_2$, 33395-22-1.

Supplementary Material Available: Listings of structure factor amplitudes for compounds **1-3** (63 pages). Ordering information is given on any current masthead page.

(32) (a) King, R. B.; Ikai, S. *Inorg. Chem.* **1979**, *18*, 949. (b) Kettle, S. F.; Gowling, E. W. *Ibid.* **1964**, *3*, 604. (c) Olander, W. K.; Brown, T. L. *J. Am. Chem. Soc.* **1972**, *94*, 2139.

(33) Lillya, C. P.; Dobosh, P., private communication.

Alkane Dehydrogenation by Iridium Complexes

Robert H. Crabtree,* Michelle F. Mellea, Jean M. Mihelcic, and Jennifer M. Quirk

Contribution from the Yale University Department of Chemistry, Sterling Chemistry Laboratory, New Haven, Connecticut 06511. *Received May 8, 1981*

Abstract: Cyclopentene reacts with $IrH_2S_2L_2^+$ at 40 °C (S = H_2O or acetone; L = PPh_3) to give $CpIrHL_2^+$. The same product is formed from cyclopentane at 80 °C in the presence of 3,3-dimethyl-1-butene (**5**). Cyclooctene or cyclooctane and **5** give Ir(1,5-cyclooctadiene)L_2^+. Evidence against colloid, radical, or carbonium ion mechanisms is given. We propose that this system constitutes the first example of a reverse hydrogenation of an alkane by a transition-metal complex.

The activation of alkanes by soluble transition-metal species has been the object of much study.[1] After a brief review of some of this work, we will discuss our own approach, which has led to the development of a system in which a variety of alkanes can be dehydrogenated to give π-coordinated ligands.

Much work has gone into attempting to activate alkanes via eq 1 with nucleophilic metal fragments. The hope has been that the metal will cleave an alkane CH bond by an "oxidative" addition. As the driving force for additions of this type has been

$$M + \gtrdot C{-}H \rightarrow \gtrdot C{-}M{-}H \qquad (1)$$

thought to be the dispersal of negative charge from the metal to the alkyl and hydride ligands, a nucleophilic metal has generally been considered as the best type of candidate for the reaction. In this connection, Chatt[2] et al. and Ittel[3] et al. have studied $Mdmpe_2$ (M = Fe, Ru, or Os; dmpe = 1,2-dimethylphosphinoethane), generated thermally from $MArHdmpe_2$, and Green[4] et al. have studied "Cp_2W" (Cp = cyclopentadienyl), generated photochemically from Cp_2WH_2. The ruthenium-based system is successful in activating CH bonds in free arenes, in the coordinated dmpe group, or in free CH_3CN and $(CH_3)_2CO$. The tungsten system activates phenyl and benzylic CH bonds in arenes and the CH bonds of $Si(CH_3)_4$. None of these systems, however, has been reported to activate free alkanes.

A number of systems[5] based on simple salts of Pt and Ir are known to catalyse H/D exchange in alkanes, although there is some question as to whether or not the active species in these solutions is homogeneous.[6]

Radicals can abstract hydrogen atoms from alkanes,[7] and a number of cases are known[8-10] where transition-metal-centered radicals or free radicals produced by transition-metal reagents give reactions of this type. The well-known Fenton's[11] reagent falls into this category.

A number of commercially important processes rely on carbonium ion rearrangements induced by Lewis-acid catalysts. These, and radical-based systems, however, offer little expectation of the sort of selectivity that might be associated with a system operating via eq 1.

We now report fully on a stoichiometric, selective, homogeneous, alkane dehydrogenation system which we propose acts via a reverse-hydrogenation mechanism, involving eq 1 as a first step. We find that an electrophilic, rather than a nucleophilic, metal center is involved. A brief note on these results has appeared.[12]

Baudry, Ephritikine, and Felkin have recently reported a similar system to ours, only based on rhenium;[13] it may well be mechanistically related.

Results and Discussion

The Nature of the Problem: A Comparison with Hydrogenation. The conversion of alkanes to alkenes can be regarded as the reverse of the well-known alkene hydrogenation reaction:

$$H_2 + \rightleftharpoons \underset{\text{dehydrogenation}}{\overset{\text{hydrogenation}}{\rightleftharpoons}} H\diagup\!\!\diagdown H \qquad (2)$$

Any catalyst for the forward process should also speed up the rate of the reverse reaction and might be considered as a potential candidate for alkane dehydrogenation. The thermodynamics of the process ($\Delta H \approx -33$ kcal/mol) shows that the "equilibrium" vastly favors the alkane side. Since the entropy of the process is negative, there should be a temperature at which the equilibrium begins to favor the alkene side. Indeed, the commerically important reforming process, e.g.,

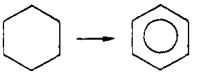

$$+ \ 3H_2 \qquad (3)$$

is catalysed by metals such as Pt, Re, or Ir, that are hydrogenation catalysts, and a high temperature (e.g., 500 °C) is required.[14] We sought to avoid the need for high temperatures in the system we

(1) Parshall, G. W. *Catalysis* **1977**, *1*, 335.
(2) Chatt, J; Davidson, J. M. *J. Chem. Soc.* **1965**, 843.
(3) Ittel, S. D.; Tolman, C. A.; Jesson, J. P. *Adv. Chem. Ser.* **1979**, *173*, 67.
(4) Green, M. L. H. *Pure Appl. Chem.* **1978**, *50*, 27.
(5) (a) Gol'dshleger, N. F.; Tyabin, M. B.; Shilov, A. E.; Shteinman, A. A.; *Zh. Fiz. Khim.* **1969**, *43*, 2174. (b) Garnett, J. H.; Long, M. A.; Peterson, K. B. *Aust. J. Chem.* **1974**, *27*, 1823.
(6) Cotton, F. A.; Wilkinson, G. W. "Advanced Inorganic Chemistry", 4th ed.; Wiley: New York, 1980; p 1245. Parshall, G. W. "Homogeneous Catalysis", 1st ed.; Wiley: New York, 1980, p 179.
(7) Norman, R. O. C. "Principles of Organic Synthesis"; Methuen: London, 1968; p 471.
(8) Hill, C. L.; Schardt, B. C. *J. Am. Chem. Soc.* **1980**, *102*, 6374.
(9) Sofranko, J. A.; Eisenberg, R.; Kampmeier, J. A. *J. Am. Chem. Soc.* **1980**, *102*, 1163.
(10) Chang, C. K.; Juo M. S. *J. Am. Chem. Soc.* **1979**, *101*, 3413.
(11) Fenton, H. S. H. *J. Chem. Soc.* **1894**, *65*, 899.
(12) Crabtree, R. H.; Mihelcic, J. M.; Quirk, J. M. *J. Am. Chem. Soc.* **1979**, *101*, 7738.
(13) Baudry, D.; Ephritikine, M.; Felkin, H. *Chem. Commun.* **1980**, 1243.
(14) Paal, Z. *Adv. Catal.* **1980**, *29*, 273.

0002-7863/82/1504-0107$01.25/0